Research Square

Preprints are preliminary reports that have not undergone peer review.
They should not be considered conclusive, used to inform clinical practice,
or referenced by the media as validated information.

EP300 promotes macrophage M2 polarization in diffuse large B-cell lymphoma through the NF-κB/CXCR4 axis

Xinxia Li

lxx-patho@163.com

Xinjiang Medical University Affiliated Tumor Hospital

Cancan Wang

Xinjiang Medical University Affiliated Tumor Hospital

Ning Feng

Xinjiang Medical University Affiliated Tumor Hospital

Lichao Jiao

Xinjiang Medical University Affiliated Tumor Hospital

Junlong He

Xinjiang Medical University Affiliated Tumor Hospital

Man Wu

Xinjiang Medical University Affiliated Tumor Hospital

Article

Keywords:

Posted Date: October 30th, 2026

DOI: https://doi.org/10.21203/rs.3.rs-11205143/v1

License: This work is licensed under a Creative Commons Attribution 4.0 International License.
Read Full License

Additional Declarations: (Not answered)

EP300 promotes macrophage M2 polarization in diffuse large B-cell lymphoma through the NF-κB/CXCR4 axis

Cancan Wang[1,2†], Feng Ning[1†], Lichao Jiao[1†], Junlong He[1], Man Wu[1], and Xinxia Li[1*]

[1]Department of Pathology, Xinjiang Medical University Affiliated Tumor Hospital, Urumqi 830000, Xinjiang, China
[2]Department of oncology, Chongqing University Fuling Hospital, Fuling 408000, Chongqing, China

Cancan Wang[1,2†], Feng Ning [1†] and Lichao Jiao [1†] These authors have contributed equally to this work.

*Correspondence:
Xinxia Li, Email: lxx-patho@163.com
Keywords: Diffuse large B-cell lymphoma (DLBCL); EP300/p300; NF-κB; CXCR4; Macrophage M2 polarization

ABSTRACT

Diffuse large B-cell lymphoma (DLBCL) is the most common aggressive non-Hodgkin lymphoma, and the immunosuppressive tumor microenvironment (TME) contributes to its progression and chemoresistance. EP300 (p300) is a histone acetyltransferase and general transcriptional coactivator that is recurrently dysregulated in B-cell lymphomas, yet its role in shaping the DLBCL immune microenvironment remains unclear. Here we show that EP300 is overexpressed in DLBCL and that high EP300 expression correlates with poor overall survival. CRISPR/Cas9-mediated knockout of EP300 in DLBCL cells suppressed proliferation, promoted apoptosis, and inhibited subcutaneous xenograft growth. Integrative label-free quantitative proteomics and RNA sequencing revealed that EP300 knockout globally suppressed immune-related pathways, most prominently NF-κB signaling, and identified CXCR4 as the sole membrane receptor consistently downregulated at both the protein and mRNA levels. Mechanistically, EP300 knockout reduced phosphorylation of p65 and IκBα, decreased expression of the NF-κB target gene CXCR4 and of the M2-polarizing cytokines CSF1, CCL2 and IL-10, and diminished their secretion. Conditioned-medium and co-culture experiments demonstrated that these EP300-dependent soluble factors shape macrophage polarization: EP300 knockout shifted macrophages toward a CD86-high/CD206-low phenotype, and this effect showed cell-context dependence. Collectively, these findings identify an EP300–NF-κB–CXCR4 axis that sustains an M2-polarized microenvironment in DLBCL and nominate EP300 as a candidate therapeutic target for high-EP300 DLBCL.

1. Introduction

Diffuse large B-cell lymphoma (DLBCL) is the most common aggressive non-Hodgkin lymphoma, accounting for 30–40% of cases, and is characterized by marked molecular and clinical heterogeneity [1-3]. Although rituximab-based immunochemotherapy (R-CHOP) achieves long-term remission in approximately 60% of patients, 30–40% relapse or become refractory and have a poor prognosis [1]. The tumor microenvironment (TME) is a major determinant of DLBCL progression and drug resistance, and gene-expression-derived stromal signatures correlate with patient outcome [4, 5]. Tumor-associated macrophages (TAMs) are among the most abundant immune cells in the TME and can polarize toward a pro-inflammatory, anti-tumoral M1 phenotype or an anti-inflammatory, pro-tumoral M2 phenotype [6, 7]. M2 TAMs promote tumor progression and immune evasion, and their high infiltration correlates with poor prognosis in DLBCL [8, 9]. Macrophage M2 polarization is largely driven by tumor-cell-derived signals: CSF1, CCL2 and IL-10 are key M2-polarizing cytokines [8], and tumor-derived metabolites such as lactate can directly instruct M2 polarization [10]. However, the signaling pathways through which tumor cells upregulate the expression and secretion of these factors are incompletely understood.

EP300 (also known as p300) is a histone acetyltransferase (HAT) and general transcriptional coactivator that acetylates histones and opens chromatin to sustain gene transcription [11, 12]. EP300 is one of the most frequently mutated epigenetic regulators in DLBCL; Huang and colleagues reported that CREBBP/EP300 mutations upregulate CCL2/CSF1 through the FBXW7–NOTCH pathway to promote macrophage M2 polarization and tumor progression [13, 14]. Notably, loss-of-function mutation is not equivalent to wild-type overexpression: in many cancers EP300 is overexpressed and promotes proliferation and progression [12, 15], indicating context-dependent functions. In addition, p300 was recently implicated as a histone lactylation writer [16, 17], suggesting that EP300 may also regulate gene expression through lactylation. Whether wild-type, overexpressed EP300 promotes DLBCL progression by shaping macrophage polarization has remained unclear.

Nuclear factor-κB (NF-κB) signaling is constitutively active in DLBCL and is a core driver of tumor progression [18]. As a key coactivator of p65, EP300 promotes transcription of NF-κB target genes by acetylating p65 and histones at target loci [19, 20], including the chemokine receptor CXCR4 and M2-polarizing cytokines such as CCL2 [21, 22]. This suggests that EP300 may sustain NF-κB activity to promote secretion of M2-polarizing factors and thereby drive macrophage polarization in the TME; however, this hypothesis had not been tested experimentally.

Here, by integrating label-free quantitative proteomics, transcriptomics and functional assays, we systematically dissect the role and mechanism of EP300 in DLBCL. We show that EP300 is overexpressed in DLBCL and associated with poor prognosis; that EP300 knockout reduces NF-κB pathway activity and CXCR4 expression, decreases secretion of the M2-polarizing cytokines CSF1, CCL2 and IL-10, and shifts macrophages toward a CD86-high/CD206-low phenotype, ultimately

inhibiting tumor growth. These results identify a novel EP300–NF-κB–CXCR4 axis that shapes macrophage polarization and provide a potential therapeutic target for DLBCL.

2. Results

2.1 EP300 is overexpressed in DLBCL and correlates with poor prognosis

We first analyzed the functional dependency of EP300 in DLBCL using public databases. CRISPR screening data from DepMap 24Q4 showed that EP300 knockout significantly impaired cell fitness in 19 DLBCL cell models (Fig. 1A), indicating that EP300 is a dependency gene in DLBCL cells; in two independent cohorts, patients with high EP300 expression had significantly shorter overall survival (OS) than those with low expression (Fig. 1B). Further validation at the tissue level: immunohistochemistry (IHC) showed that EP300 expression scores were significantly higher in DLBCL tissues (n = 154) than in reactive lymphoid hyperplasia (RLHN, n = 93) (Fig. 1C, D), and the proportion of high EP300 expression was significantly higher in DLBCL than in RLHN (68.83% vs 27.96%; Table 1).

We further analyzed the association between EP300 expression and clinicopathological features. High EP300 expression was significantly associated with extranodal involvement, the non-GCB/ABC phenotype, and a reduced absolute lymphocyte count (Table 2; Supplementary Fig. S1A), whereas no significant association was observed for age, sex, Ann Arbor stage, IPI score, B symptoms, LDH, ANC, AMC, or Ki-67 (Table 2; Supplementary Fig. S1A). In our cohort of 154 patients, those with high EP300 expression (n = 106) had significantly shorter OS than those with low expression (n = 48) (Fig. 1E), and progression-free survival (PFS) was also significantly shorter (Fig. 1F). Univariate Cox regression showed that high EP300 expression was associated with poor OS and PFS; high $CD163^+$ TAM infiltration was associated with poor OS and PFS, whereas high $CD68^+CD163^+$ TAM infiltration was associated only with poor OS (Fig. 1G, H). Multivariate Cox analysis, adjusting for the indicated clinicopathological covariates, showed that high EP300 expression remained an independent adverse prognostic factor for OS, as did age ≥60 years and high $CD163^+$ TAM infiltration; high EP300 expression was not independently associated with PFS (Fig. 1I, J). Together, these data establish that EP300 is overexpressed in DLBCL and is independently associated with poor OS.

2.2 EP300 knockout inhibits DLBCL cell proliferation, promotes apoptosis and suppresses xenograft growth

To assess the biological function of EP300, we first verified its high expression in DLBCL tissues: Western blot showed that p300 protein levels (p300/ACTB ratio) were significantly higher in 7 DLBCL tissues (D1#–D7#) than in 7 reactive hyperplasia tissues (R1#–R7#) (Fig. 2A, C), consistent with the immunohistochemistry results. Subsequently, we constructed EP300-KO cell lines in OCI-LY3 (ABC) and Pfeiffer (GCB) cells using CRISPR-Cas9 technology, and Western blot confirmed the loss of p300 protein expression (Fig. 2B, D, E; Supplementary Fig. S2A, B). Functionally, CCK-8 assays showed that EP300-KO significantly inhibited proliferation of both cell

lines at 24, 48 and 72 h (Fig. 2F, G); EdU incorporation assays showed decreased DNA synthesis activity (Fig. 2H, I); Annexin V-FITC/PI double staining showed a significant increase in apoptotic cell proportion (Fig. 2J–L; flow cytometry gating and staining controls in Supplementary Fig. S2C–H, S3A–H). In the OCI-LY3 subcutaneous xenograft model (n = 6/group), EP300-KO significantly attenuated tumor growth, with reduced terminal tumor weight (Fig. 2M–O) and decreased Ki67 positivity in xenograft tumors (Fig. 2P; Supplementary Fig. S3I). Together, EP300-KO inhibits DLBCL cell proliferation, induces apoptosis and suppresses in vivo tumorigenesis.

2.3 Transcriptomic and proteomic analyses reveal molecular remodeling and reduced immune-related programs upon EP300 knockout

To dissect the molecular changes upon EP300 loss, we performed RNA sequencing and label-free quantitative proteomics in EP300-KO and control OCI-LY3 cells (n = 3 per group; Supplementary Fig. S4A). A total of 15,487 genes and 8,313 proteins were quantified, and PCA separated the two groups in both datasets (Supplementary Fig. S4B–G).

Differential analysis identified 2,495 differentially expressed genes at the RNA level and 146 differentially expressed proteins at the protein level (Fig. 3A, B). Integration revealed 54 molecules that met the differential screening criteria at both the protein and mRNA levels, including the chemokine receptor CXCR4, whose protein and mRNA levels were both significantly downregulated (Fig. 3C, D); $\log_2$FC values at the two levels showed only weak positive correlation (Fig. 3E).

Gene set enrichment analysis (GSEA) showed that immune-related Hallmark gene sets were consistently negatively enriched at the RNA level, while angiogenesis, myogenesis and MYC target gene sets were positively enriched (Fig. 3G); the 7 nominally significant Hallmark gene sets at the protein level were also all negatively enriched, and the enrichment scores at the two levels showed low overall correlation (Fig. 3F). KEGG analysis was dominated by negatively enriched pathways, with mismatch repair and T-cell receptor signaling pathways positively enriched (Supplementary Fig. S4H–J). A heatmap of representative genes showed broad changes in glycolysis, chemokine, cell-cycle and apoptosis-related genes upon EP300-KO (Fig. 3H). These results direct the downstream effects of EP300 to NF-κB-related signaling and immunoregulatory secretory programs in tumor cells.

2.4 EP300-KO reduces NF-κB-related signaling and macrophage-modulatory secretory factors and impairs chemotactic response

Based on the multi-omics results, we first verified NF-κB pathway activity in OCI-LY3 cells. Compared with controls, EP300-KO cells showed significantly reduced p-p65/p65 and p-IκBα/IκBα ratios, and CXCR4 protein levels were also significantly decreased (Fig. 4A–F). qRT-PCR showed consistent downregulation of NF-κB downstream target genes (Fig. 4G). ELISA further confirmed that secretion levels of CCL2, IL-10 and M-CSF in conditioned medium from EP300-KO cells were all significantly decreased (Fig. 4H), indicating that EP300 knockout reshapes the immunoregulatory secretory profile of tumor cells.

To assess the functional consequences of secretome changes, we pretreated THP-1-derived macrophages with conditioned medium from control or EP300-KO cells for 48 h, then seeded the same number of cells in the upper chamber of a Transwell, with CXCL12 in the lower chamber to assess chemotactic ability. Compared with control conditioned medium, macrophages pretreated with EP300-KO conditioned medium showed significantly reduced migration (Fig. 4I, J), indicating that EP300 knockout in tumor cells can impair macrophage chemotactic response to CXCL12 by altering the secretome.

2.5 EP300-KO cell conditioned medium induces macrophage surface marker remodeling

To assess the effect of tumor cell secretome changes on macrophage phenotype, we treated PMA-induced THP-1-derived macrophages with conditioned medium from control or EP300-KO cells for 48 h, and detected surface markers by flow cytometry (Fig. 5A; gating strategy and staining controls in Supplementary Fig. S6). In the OCI-LY3 system, macrophages treated with EP300-KO conditioned medium exhibited a CD86-high/CD206-low phenotype (Fig. 5B, C; Supplementary Fig. S5B), indicating that the secretome of EP300-KO tumor cells can induce macrophage surface marker remodeling. In the Pfeiffer system, EP300-KO conditioned medium also induced changes in macrophage surface marker distribution, but with smaller magnitude and a different pattern from the OCI-LY3 system (Supplementary Fig. S5C, D), suggesting that the strength and pattern of this phenotypic effect are influenced by tumor cell background.

We performed multiplex immunofluorescence co-staining of EP300, CD68 and CD163 in 154 DLBCL patient tissues (Fig. 5D). $CD163^+$ macrophage infiltration was significantly higher in EP300-high tissues than in EP300-low tissues (Fig. 5D). "Correlation analysis showed that EP300 expression was positively correlated with $CD163^+$ and $CD68^+CD163^+$ macrophage density, but not with total $CD68^+$ cell density (Fig. 5E; Table 3), indicating that EP300 expression is specifically associated with M2-like macrophage infiltration.

2.6 Schematic diagram of the EP300–NF-κB–CXCR4 axis in macrophage M2 polarization in DLBCL

Integrating cellular, molecular and tissue analyses, we propose a working model based mainly on the OCI-LY3 results (Fig. 6): EP300 knockout attenuates NF-κB-related signaling and decreases secretion of M-CSF, CCL2 and IL-10 in tumor cells, thereby impairing macrophage chemotactic response to CXCL12 and inducing a CD86-high/CD206-low phenotype. The weak positive correlation between EP300 expression and $CD163^+$/$CD68^+CD163^+$ cell density in 154 DLBCL tissues corroborates these cell-based findings at the tissue level.

This model connects tumor cell-intrinsic EP300 programs to tumor–macrophage crosstalk. However, the divergent phenotypic changes observed in Pfeiffer cells define the limits of this model, and the complete causal chain awaits confirmation by pathway rescue experiments.

3. Discussion

By integrating clinical cohorts, multi-omics, cellular and animal experiments, this study delineates the role and mechanism of EP300 in DLBCL. Public CRISPR screening data identify EP300 as a dependency gene in DLBCL cell models, and its high expression is associated with poor prognosis; its knockout suppresses DLBCL cell proliferation, promotes apoptosis and attenuates xenograft growth. Multi-omics analysis reveals a global repression of immune-related pathways, most prominently NF-κB, upon EP300 loss. Mechanistically, EP300 knockout reduces phosphorylation of p65 and IκBα, downregulates the NF-κB target CXCR4 and the M2-polarizing cytokines CSF1, CCL2 and IL-10, and thereby shifts macrophages toward a CD86-high/CD206-low phenotype. These results define an EP300–NF-κB–CXCR4 axis that links aberrant epigenetic regulation in DLBCL to the establishment of an immunosuppressive microenvironment.

Recent work showed that CREBBP/EP300 mutations upregulate CCL2/CSF1 through the FBXW7–NOTCH pathway to promote macrophage M2 polarization in the DLBCL microenvironment [14]. Notably, the functional evidence for macrophage polarization in that study derives mainly from CREBBP-mutant models, and EP300 mutations in DLBCL are frequently hypomorphic, impairing only catalytic activity [13]—distinct from the complete loss elicited by CRISPR/Cas9 knockout in our system. In both DLBCL cell lines, we observed significant downregulation of M-CSF and IL-10 secretion, indicating that in the context of wild-type EP300 overexpression, EP300 primarily sustains NF-κB activity to regulate transcription and secretion of M2-polarizing cytokines. Together, these studies suggest that CREBBP/EP300 regulation of the DLBCL microenvironment is context-dependent and that therapeutic targeting of this family requires careful patient stratification.

We identified CSF1, CCL2 and IL-10 as key secreted effectors downstream of the EP300–NF-κB axis. These cytokines have non-redundant roles in M2 polarization: CSF1 is a master regulator of macrophage differentiation and survival, and CSF1/CSF1R blockade markedly reduces intratumoral macrophages [23]; CCL2 recruits circulating monocytes to tumors, thereby governing TAM replenishment [8]; and IL-10 is a principal executor of M2 immunosuppressive function [7]. EP300 knockout significantly reduced secretion of these cytokines, with M-CSF and IL-10 downregulation consistent across both cell lines; conditioned-medium transfer experiments confirmed that this regulation is mediated by soluble tumor-derived factors rather than cell–cell contact. At the tissue level, EP300 expression correlated weakly and positively with $CD163^+$ and $CD68^+CD163^+$ cell density, but not with total $CD68^+$ cell density; multivariate survival analysis showed that high EP300 expression and $CD163^+$ TAM level are both independent adverse prognostic factors for OS. These in vitro and in vivo findings corroborate each other, indicating that the effect of EP300 knockout is, in essence, a remodeling of the tumor secretome, which is therapeutically tractable.

Beyond secreted factors, this study also suggests two mechanistic leads awaiting

validation. First, CXCR4 is the only membrane receptor consistently downregulated at both the protein and mRNA levels in our multi-omics analysis, and is also a known NF-κB target gene [21]; its downregulation suggests that EP300 knockout may impair the chemotactic response of tumor cells to microenvironmental CXCL12 [24, 25], and its exact function awaits confirmation by rescue experiments. Second, EP300 has been reported to possess histone lactylation writer function [16, 17], and our transcriptomic data showed concordant upregulation of glycolytic genes (LDHA, ENO1, HK2) upon EP300 knockout; given that tumor-derived lactate can directly drive macrophage M2 polarization [10] and that histone lactylation participates in tumorigenesis and macrophage function regulation [26, 27], whether EP300 participates in the transcriptional regulation of M2-polarizing cytokine gene loci through lactylation awaits validation by locus-specific chromatin studies (e.g., H3K18la CUT&Tag/ChIP-seq).

Our findings have potential translational value. Small-molecule inhibitors of EP300/CBP show preclinical activity in hematologic malignancies [28], and the EP300/CBP bromodomain inhibitor CCS1477 (inobrodib) inhibits DLBCL growth [29]. Recent therapeutic advances, including the antibody–drug conjugate polatuzumab vedotin [30] and the bispecific antibody glofitamab [31], have improved outcomes in DLBCL, yet microenvironment-mediated resistance remains a challenge [32, 33]. The EP300–CSF1/CCL2 regulatory relationship revealed by this study suggests that EP300 inhibitors may synergize with TAM-targeting strategies such as CSF1R blockade [23, 34], and epigenetic inhibitors can themselves reprogram TAMs toward an anti-tumoral state [35]. Moreover, CXCR4 antagonists are already clinically approved [25], so combined targeting of EP300 and CXCR4 is, in principle, rapidly translatable once the functional role of CXCR4 is confirmed.

This study has several limitations. First, the nude-mouse xenograft model lacks a complete adaptive immune system, so the impact of the EP300–NF-κB axis on T-cell immunity must be confirmed in immunocompetent models. Second, direct CXCR4 rescue validation and dissection of the FBXW7–NOTCH branch remain to be performed. Third, the macrophage phenotype readout is based on CD86/CD206 surface markers, and its correspondence to the functional state represented by intratumoral CD163 remains to be clarified. Finally, the correlation between EP300 and $CD163^{+}$ cell density at the tissue level is weak and observational, and the causal direction awaits validation in larger cohorts. Notwithstanding these limitations, this study establishes a key role for EP300 in maintaining the immunoregulatory secretory program of DLBCL cells through NF-κB signaling and provides a mechanistic basis and potential target for epigenetic therapy of high-EP300 DLBCL.

5. Materials and Methods

5.1 Patient specimens

DLBCL tumor tissues (n = 154) and reactive hyperplastic lymph nodes (n = 93) were collected from the Affiliated Tumor Hospital of Xinjiang Medical University. The study was approved by the ethics committee of the Affiliated Tumor Hospital of Xinjiang

Medical University (approval no. G-2023007), and informed consent was obtained from all patients in accordance with the Declaration of Helsinki. All specimens were independently confirmed by two pathologists. 154 DLBCL patients were included in survival analysis, with follow-up until May 18, 2025. Multiplex immunofluorescence analysis included patients with complete tissue microarray sections and follow-up data.

5.2 Cell culture and generation of EP300 knockout cell lines

Human DLBCL cell lines OCI-LY3 (ABC subtype) and Pfeiffer (GCB subtype) were purchased from Wuhan Procell Life Science & Technology Co., Ltd., and THP-1 was purchased from the Cell Bank of the Chinese Academy of Sciences (catalog no. TCHu 57). OCI-LY3 and Pfeiffer cells were cultured in RPMI-1640 medium supplemented with 10% fetal bovine serum (FBS) and 1% penicillin–streptomycin; THP-1 cells were cultured in specialized complete medium (MD61). Cell line identity was confirmed by STR profiling, and cultures were routinely tested negative for mycoplasma. Single-guide RNAs (sgRNAs) targeting EP300 were cloned into the lentiCRISPR v2 vector, with empty vector as control. After transient transduction, cells were selected with 3 μg/mL puromycin for 3 rounds; control cells were designated as CTR, and knockout cells as EP300-KO, with knockout efficiency verified by Western blot. The sgRNA sequences targeting EP300 are listed in Supplementary Table 1.

5.3 Public data and survival analysis

CRISPR dependency data for DLBCL cell models were obtained from DepMap 24Q4 Public, and EP300 gene effect scores (Chronos) were analyzed (n = 19 models). In the GSE10846 (n = 420) and GSE181063 (n = 1,170) cohorts, patients were divided into high and low EP300 expression groups by the median, and survival was analyzed by the Kaplan–Meier method with univariate and multivariate Cox regression (covariates including age and IPI score; proportional hazards assumption verified by Schoenfeld residual tests). Variable selection used LASSO regression with 10-fold cross-validation. Samples with missing data were excluded, and all analyses were performed in R 4.3.2.

5.4 **Proteomics, RNA sequencing and bioinformatics analysis**

Control and EP300-KO OCI-LY3 cells (n = 3 per group) were subjected to DIA proteomics (Genewiz): proteins were digested with SP3 magnetic beads and analyzed by LC-MS/MS (Orbitrap Astral Zoom). Data were searched against the UniProt human protein database using DIA-NN, and differential proteins were screened with $|\log_2 FC| > 0.585$ and Benjamini–Hochberg-adjusted $P < 0.05$ (PRIDE: PXD084097). Total RNA was extracted with magnetic beads, and strand-specific libraries were constructed and sequenced (150 bp paired-end) on NovaSeq 6000, aligned to GRCh38. Differentially expressed genes were identified with DESeq2 ($|\log_2 FC| > 0.585$, adjusted $P < 0.05$) (GEO: GSE347127). GSEA was performed with gseapy (MSigDB Hallmark), and GO and KEGG enrichment analyses were performed with GOSeq and hypergeometric tests, respectively. Proteome–transcriptome integration used Pearson correlation, four-quadrant scatter plots and screening of concordant differentially expressed genes.

5.5 Western blot

Cells were lysed in RIPA buffer containing protease and phosphatase inhibitors, quantified by BCA assay, resolved by SDS-PAGE and transferred to PVDF membranes, which were blocked with 5% non-fat milk. Primary antibodies included p300 (D2X6N, CST, #54062), phospho-NF-κB p65 (Ser536) (93H1, CST, #3033), NF-κB p65 (D14E12, CST, #8242), phospho-IκBα (Ser32) (14D4, CST, #2859), IκBα (44D4, CST, #4812), CXCR4 (D4Z7W, CST, #6670), all at 1:1,000; β-actin (HUABIO, R1207-1, 1:20,000) served as loading control. After overnight incubation at 4 °C, HRP-conjugated secondary antibodies were applied, and signals were visualized by ECL and quantified with ImageJ; phosphorylated proteins were normalized to their corresponding total proteins, and other proteins to β-actin.

5.6 qPCR and ELISA

Total RNA was extracted with TRIzol and reverse-transcribed to cDNA, and relative expression of CXCR4, CSF1, CCL2, IL10, BCL2 and ICAM1 was detected by SYBR Green, with ACTB as internal control, calculated by the 2^(-ΔΔCt) method; primer sequences are listed in Supplementary Table 1. Conditioned medium was collected from control and EP300-KO cells after 48 h culture, and Human CSF1/M-CSF, CCL2/MCP-1 and IL-10 were measured with ELISA kits (Elabscience, E-EL-H0097, E-EL-H6005, E-EL-H6154), with 3 independent biological experiments, each with 6 technical replicates.

5.7 Cell proliferation and apoptosis assays

For CCK-8 assays, cells were seeded and CCK-8 reagent was added, and absorbance at 450 nm was measured at 0, 24, 48 and 72 h. Proliferation was additionally assessed by EdU incorporation (4 h labeling) followed by flow cytometry. Apoptosis was assessed by Annexin V-FITC/PI double staining and analyzed by flow cytometry. Cell proliferation and apoptosis experiments were each performed in 3 independent replicates.

5.8 Macrophage conditioned-medium treatment

THP-1 cells were differentiated into macrophages with 100 nM PMA for 48 h, and some were additionally treated with 20 ng/mL IL-4 and IL-13 for 48 h for M2 polarization. Macrophages were treated with 48 h conditioned medium from control or EP300-KO cells for 48 h, followed by flow cytometry or chemotaxis assay: for flow cytometry, cells were Fc-blocked and stained with CD86-PE (BioLegend, 374206) and CD206-APC (BioLegend, 321110), using a standardized gating and compensation strategy (Supplementary Fig. S6), and analyzed with FlowJo; $CD86^+$ cells were defined as Q1+Q2, and $CD206^+$ cells as Q2+Q3. For the chemotaxis assay, macrophages pretreated with conditioned medium were seeded in the upper chamber of a Transwell (8 μm pores) at 2×10^4 per well, with CXCL12 (100 ng/mL) in the lower chamber for 6 h, and migrated cells on the lower side of the membrane were counted.

5.9 Flow cytometry

Macrophages treated with conditioned medium were Fc-blocked and stained with CD86-PE and CD206-APC. All experiments used a standardized gating and compensation strategy (FSC/SSC gating, doublet exclusion, Live/Dead exclusion,

single-stain controls) (Supplementary Fig. S6). Cells were acquired on a flow cytometer and analyzed with FlowJo; $CD86^+$ cells were defined as Q1+Q2, and $CD206^+$ cells as Q2+Q3.

5.10 Immunohistochemistry and multiplex immunofluorescence

Paraffin sections were deparaffinized, rehydrated and subjected to antigen retrieval. For IHC, primary antibodies (EP300, Ki67) were applied, followed by DAB detection and hematoxylin counterstain. For multiplex immunofluorescence, tissue sections from 154 DLBCL patients were stained with DAPI, CD68, CD163 and EP300 antibodies, and images were acquired to quantify EP300 mean fluorescence intensity (MFI) and $CD68^+$, $CD163^+$ and $CD68^+CD163^+$ cell densities; patients were divided into high and low expression groups by the median EP300 MFI (114.59) (n = 77 each).

5.11 Subcutaneous xenograft model

BALB/c nude mice (4–6 weeks old, female, n = 6 per group) were injected subcutaneously with 1×10^7 control or EP300-KO OCI-LY3 cells. Tumor volume was measured every 2 days from day 14 to day 26, calculated as $V = L \times W^2/2$. At endpoint, mice were euthanized, and tumors were excised, weighed and paraffin-embedded for IHC. All animal experiments were approved by the Xinjiang Medical University IACUC (approval no. IACUC-20230307-7), and the maximum permissible tumor burden was not exceeded.

5.12 Statistical analysis

Data are presented as mean ± SD and were analyzed with GraphPad Prism and R. Two-group comparisons used two-tailed unpaired Student's t-test; comparisons with non-normal distribution or small sample size used Mann–Whitney U test or Wilcoxon rank-sum test; growth curves were compared by two-way ANOVA; survival was analyzed by the Kaplan–Meier method and log-rank test; correlations used Spearman/Pearson correlation; and multiple testing was corrected by the Benjamini–Hochberg method. *P < 0.05, **P < 0.01, ***P < 0.001, ****P < 0.0001 were considered statistically significant.

Funding.

This work was supported by the National Natural Science Foundation of China (82360037), the Science and Technology Leading Talent Project of Tianshan Talents Program (2024TSYCLJ0025), the Xinjiang Higher Education Institution Enterprise Joint Project for Talent Development and Key Scientific Research Breakthroughs (XJMU2026G011), the National Natural Science Foundation of China (8266010264), and the State Key Laboratory of Neurology and Oncology Drug Development (SLKSIM-20250115).

Author contributions.

CW designed the experiments, analyzed the data, and drafted the original manuscript; NF contributed to conceptualization, data curation, formal analysis, investigation, methodology, software, validation, visualization, and writing – original draft; LJ contributed to data curation, formal analysis, investigation, methodology, software, validation, visualization, and writing – original draft; JH acquired funding and

administrated the project; MW analyzed the data, critically reviewed and revised the manuscript, and supervised the study; XL contributed to conceptualization, funding acquisition, project administration, supervision, and writing – review & editing. All authors contributed to the article and approved the final version for publication.

Competing interests.

The authors declare no competing interests.

Data availability.

The RNA-seq data have been deposited in the Gene Expression Omnibus (GEO) under accession no. GSE347127; the proteomics data have been deposited in the ProteomeXchange Consortium via the PRIDE partner repository under accession no. PXD084097. All other data supporting the findings of this study are available within the article and its Supplementary Information, or from the corresponding author upon reasonable request.

Ethics approval.

Human tissue studies were approved by the Affiliated Tumor Hospital of Xinjiang Medical University (approval no. G-2023007) and performed in accordance with the Declaration of Helsinki; informed consent was obtained from all patients. Animal experiments were approved by Xinjiang Medical University (approval no. IACUC-20230307-7); the maximum permissible tumor burden was not exceeded.

Consent for publication. The authors consent to publication.

Reference

1. Sehn LH, Salles G. Diffuse large B-cell lymphoma. N Engl J Med. 2021;384(9):842–58.
2. Schmitz R, Wright GW, Huang DW, Johnson CA, Phelan JD, Wang JQ, et al. Genetics and pathogenesis of diffuse large B-cell lymphoma. N Engl J Med. 2018;378(15):1396–407.
3. Chapuy B, Stewart C, Dunford AJ, Kim J, Kamburov A, Redd RA, et al. Molecular subtypes of diffuse large B cell lymphoma are associated with distinct pathogenic mechanisms and outcomes. Nat Med. 2018;24(5):679–90.
4. Kotlov N, Bagaev A, Revuelta MV, Phillip JM, Cacciapuoti MT, Antysheva Z, et al. Clinical and biological subtypes of B-cell lymphoma revealed by microenvironmental signatures. Cancer Discovery. 2021;11(6):1468–89.
5. Lenz G, Wright G, Dave S, Xiao W, Powell J, Zhao H, et al. Stromal gene signatures in large-B-cell lymphomas. N Engl J Med. 2008;359(22):2313–23.
6. Mantovani A, Allavena P, Marchesi F, Garlanda C. Macrophages as tools and targets in cancer therapy. Nat Rev Drug Discovery. 2022;21(11):799–820.
7. Cassetta L, Pollard JW. A timeline of tumour-associated macrophage biology. Nat Rev Cancer. 2023;23(4):238–57.
8. Sica A, Mantovani A. Macrophage plasticity and polarization: In vivo veritas. J Clin Invest. 2012;122(3):787–95.
9. Lin M, Ma S, Sun L, Qin Z. The prognostic value of tumor-associated macrophages detected by immunostaining in diffuse large B cell lymphoma: A meta-analysis.

Front Oncol. 2022;12:1094400.
10. Colegio OR, Colegio OR, Chu NQ, Szabo AL, Chu T, Rhebergen AM, et al. Functional polarization of tumour-associated macrophages by tumour-derived lactic acid. Nature. 2014;513(7519):559–63.
11. Ogryzko VV, Schiltz RL, Russanova V, Howard BH, Nakatani Y. The transcriptional coactivators p300 and CBP are histone acetyltransferases. Cell. 1996;87(5):953–9.
12. Attar N, Kurdistani SK. Exploitation of EP300 and CREBBP lysine acetyltransferases by cancer. Cold Spring Harbor Perspect Med. 2017;7(3):a026534.
13. Pasqualucci L, Dominguez-Sola D, Chiarenza A, Fabbri G, Grunn A, Trifonov V, et al. Inactivating mutations of acetyltransferase genes in B-cell lymphoma. Nature. 2011;471(7337):189–95.
14. Huang YH, Cai K, Xu PP, Wang L, Huang CX, Fang Y, et al. CREBBP/EP300 mutations promoted tumor progression in diffuse large B-cell lymphoma through altering tumor-associated macrophage polarization via FBXW7-NOTCH-CCL2/CSF1 axis. Signal Transduction Targeted Ther. 2021;6(1):10.
15. Zhu Y, Wang Z, Li Y, Peng H, Liu J, Zhang J, et al. The role of CREBBP/EP300 and its therapeutic implications in hematological malignancies. Cancers. 2023;15(4):1219.
16. Zhang D, Tang Z, Huang H, Zhou G, Cui C, Weng Y, et al. Metabolic regulation of gene expression by histone lactylation. Nature. 2019;574(7779):575–80.
17. Yi JX, Wang MW, Yu D, Zhao MQ, Wang XY, Li SQ, et al. p300-Mediated H3K18 lactylation drives radiation-induced pulmonary fibrosis via VIRMA-Dependent m^6A modification of GATA3. Adv Sci. 2026:e77328.
18. Compagno M, Lim WK, Grunn A, Nandula SV, Brahmachary M, Shen Q, et al. Mutations of multiple genes cause deregulation of NF-kappaB in diffuse large B-cell lymphoma. Nature. 2009;459(7247):717–21.
19. Gerritsen ME, Williams AJ, Neish AS, Moore S, Shi Y, Collins T. CREB-binding protein/p300 are transcriptional coactivators of p65. Proc Natl Acad Sci USA. 1997;94(7):2927–32.
20. Chen LF, Fischle W, Verdin E, Greene WC. Duration of nuclear NF-kappaB action regulated by reversible acetylation. Science. 2001;293(5535):1653–7.
21. Helbig G, Christopherson KW, Bhat-Nakshatri P, Kumar S, Kishimoto H, Miller KD, et al. NF-kappaB promotes breast cancer cell migration and metastasis by inducing the expression of the chemokine receptor CXCR4. J Biol Chem. 2003;278(24):21631–8.
22. Jin Y, Wang Y, Yang R. Chemokine ligand 2: Beyond chemotaxis-a multifaceted role in tumor progression. Front Immunol. 2025;16:1685474.
23. Ries CH, Cannarile MA, Hoves S, Benz J, Wartha K, Runza V, et al. Targeting tumor-associated macrophages with anti-CSF-1R antibody reveals a strategy for cancer therapy. Cancer Cell. 2014;25(6):846–59.

24. Bleul CC, Fuhlbrigge RC, Casasnovas JM, Aiuti A, Springer TA. A highly efficacious lymphocyte chemoattractant, stromal cell-derived factor 1 (SDF-1). J Exp Med. 1996;184(3):1101–9.
25. Cambier S, Gouwy M, Proost P. The chemokines CXCL8 and CXCL12: Molecular and functional properties, role in disease and efforts towards pharmacological intervention. Cell Mol Immunol. 2023;20(3):217–51.
26. Yu J, Chai P, Xie M, Ge S, Ruan J, Fan X, et al. Histone lactylation drives oncogenesis by facilitating m^6A reader protein YTHDF2 expression in ocular melanoma. Genome Biol. 2021;22(1):85.
27. Pan RY, He L, Zhang J, Liu X, Liao Y, Gao J, et al. Positive feedback regulation of microglial glucose metabolism by histone H4 lysine 12 lactylation in Alzheimer's disease. Cell Metab. 2022;34(4):634–48.e6.
28. Lasko LM, Jakob CG, Edalji RP, Qiu W, Montgomery D, Digiammarino EL, et al. Discovery of a selective catalytic p300/CBP inhibitor that targets lineage-specific tumours. Nature. 2017;550(7674):128–32.
29. Si RJ, Zhang YH, Hu BW, Du YX, Zou D, Wen SD, et al. The EP300-targeting drug CCS1477 inhibits the growth and development of diffuse large B-Cell lymphoma by promoting apoptosis and mitophagy to reduce drug resistance. Anti-Cancer Agents Med Chem. 2026;26(9):854–67.
30. Tilly H, Morschhauser F, Sehn LH, Friedberg JW, Trněný M, Sharman JP, et al. Polatuzumab vedotin in previously untreated diffuse large B-cell lymphoma. N Engl J Med. 2022;386(4):351–63.
31. Dickinson MJ, Carlo-Stella C, Morschhauser F, Bachy E, Corradini P, Iacoboni G, et al. Glofitamab for relapsed or refractory diffuse large B-cell lymphoma. N Engl J Med. 2022;387(24):2220–31.
32. Li X, Singhal K, Deng Q, Chihara D, Russler-Germain D, Harkins R, et al. Large B cell lymphoma microenvironment archetype profiles. Cancer Cell. 2025;43(7):1347–64.e13.
33. Xu J, Ding L, Mei J, Hu Y, Kong X, Dai S, et al. Dual roles and therapeutic targeting of tumor-associated macrophages in tumor microenvironments. Signal Transduction Targeted Ther. 2025;10(1):268.
34. Ruffell B, Coussens LM. Macrophages and therapeutic resistance in cancer. Cancer Cell. 2015;27(4):462–72.
35. Guerriero JL, Sotayo A, Ponichtera HE, Castrillon JA, Pourzia AL, Schad S, et al. Class IIa HDAC inhibition reduces breast tumours and metastases through anti-tumour macrophages. Nature. 2017;543(7645):428–32.

13. Figure legends

Fig. 1 EP300 is required for DLBCL cell fitness and correlates with poor prognosis. (a) CRISPR screening of EP300 dependency in 19 DLBCL cell models from DepMap 24Q4 (Chronos gene effect scores; more negative scores indicate stronger fitness impairment upon EP300 knockout; 0 and −1 denote non-essential and common-

essential genes). (b) Kaplan–Meier overall survival (OS) by EP300 expression in two independent cohorts. (c) Representative IHC of EP300 in reactive lymphoid hyperplasia (RLHN) and DLBCL tissues; scale bars, 50 μm. (d) Quantification of EP300 IHC scores in RLHN and DLBCL tissues. (e, f) Kaplan–Meier OS (e) and progression-free survival (PFS, f) by EP300 expression in the clinical cohort. (g, h) Univariate Cox regression for OS (g) and PFS (h). (i, j) Multivariate Cox regression forest plots for OS (i) and PFS (j). Data are mean ± SD; log-rank test (e, f) or Cox regression (g–j) as indicated. ALC, absolute lymphocyte count; AMC, absolute monocyte count; ANC, absolute neutrophil count; COO, cell of origin; IPI, International Prognostic Index; LDH, lactate dehydrogenase; TAMs, tumor-associated macrophages.

Fig. 2 EP300 knockout inhibits DLBCL cell proliferation, promotes apoptosis and suppresses xenograft growth. (a) Western blot of p300 in DLBCL versus reactive hyperplasia tissues; ACTB, loading control. (b) Western blot of p300 in CTR and EP300-KO OCI-LY3 and Pfeiffer cells. (c–e) Densitometric quantification of p300/ACTB. (f, g) CCK-8 proliferation curves of OCI-LY3 (f) and Pfeiffer (g) cells. (h, i) EdU flow cytometry histograms and quantification of EdU^+ cells. (j, k) Representative Annexin V-FITC/PI flow cytometry plots. (l) Quantification of Annexin V^+ apoptotic cells. (m–o) Subcutaneous xenograft of CTR and EP300-KO OCI-LY3 cells (n = 6 per group): (m) terminal tumor photographs; (n) terminal tumor weight; (o) growth curves. (p) Representative Ki67 IHC of xenograft tumors; scale bars, 50 μm. Data are mean ± SD from n = 7 (a) or 3 independent experiments (c–l) or n = 6 mice (m–o); two-tailed unpaired Student's t-test. *P < 0.05, **P < 0.01, ***P < 0.001.

Fig. 3 Integrative multi-omics reveals molecular remodeling and reduced immune-related programs upon EP300 knockout. (a, b) Volcano plots of differentially expressed proteins (a; 146 DEPs: 88 up, 58 down) and genes (b; 2,495 DEGs: 1,199 up, 1,296 down) in EP300 knockout versus control OCI-LY3 cells. (c) Four-quadrant plot of RNA versus protein log_2FC. (d) Overlap of differentially expressed genes at the two levels (92 protein-only, 54 concordant, 2,441 RNA-only). (e) Correlation of log_2FC for 7,578 matched RNA–protein pairs. (f) Comparison of Hallmark NES between proteome and transcriptome. (g) GSEA of immune-related Hallmark gene sets at the RNA level. (h) Heatmap of protein and RNA log_2FC for representative genes in lactylation, glycolysis, macrophage phenotype, chemokine, cell-cycle and apoptosis. Data are mean ± SD from n = 3 independent experiments; $|log_2FC| > 0.585$ and adjusted $P < 0.05$ for differential screening. FC, fold change; NS, not significant.

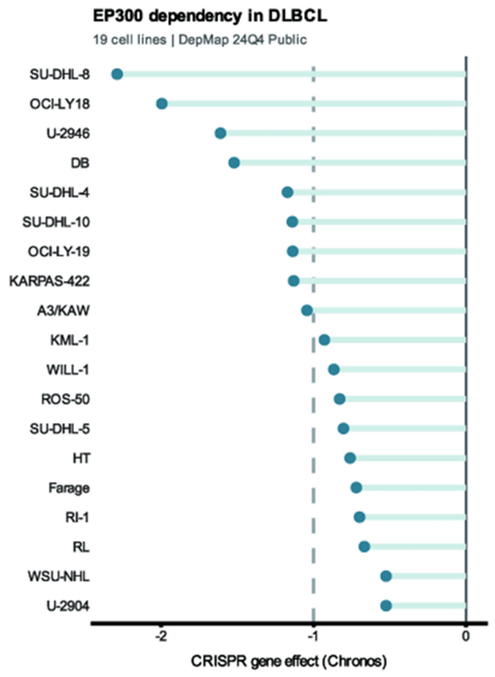
Fig. 4 EP300 knockout reduces NF-κB-related signaling and macrophage-modulatory secretory factors and impairs chemotactic response. (a–f) Western blot of p-p65/p65 (a, b), p-IκBα/IκBα (c, d) and CXCR4 (e, f) in CTR and EP300-KO OCI-LY3 cells; ACTB, loading control. (g) qRT-PCR of BCL2, ICAM1, IL10, CSF1, CXCR4 and CCL2. (h) ELISA of CCL2, IL-10 and M-CSF in conditioned medium. (i, j) Transwell chemotaxis assay: THP-1 macrophages pretreated with CTR or EP300-

KO conditioned medium, seeded in the upper chamber with CXCL12 in the lower chamber; scale bars, 100 μm. Data are mean ± SD from n = 3 independent experiments (a–g, i, j) or 3 independent experiments with 6 technical replicates each (h); two-tailed unpaired Student's t-test. *P < 0.05, **P < 0.01, ***P < 0.001, ****P < 0.0001.

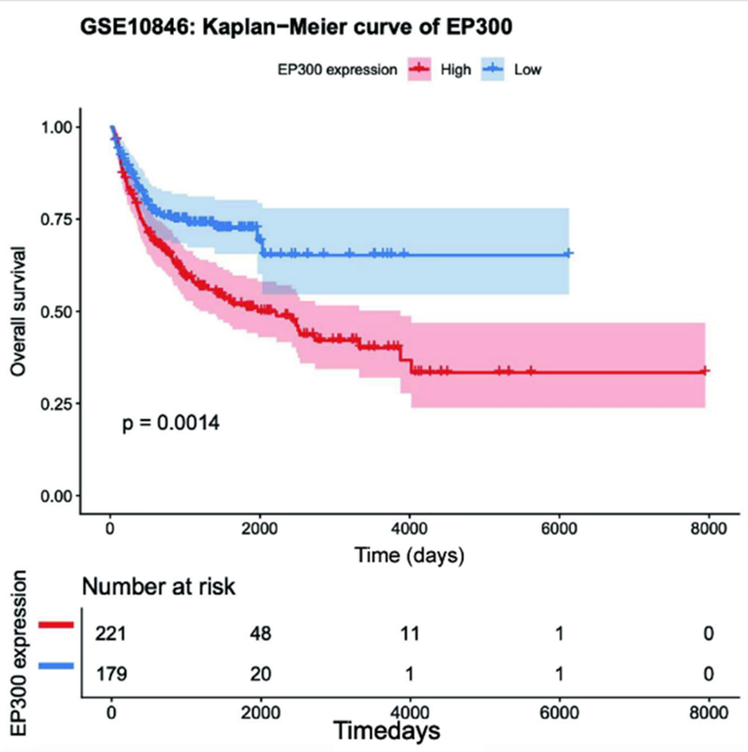
Fig. 5 EP300 knockout induces macrophage surface marker remodeling and tissue EP300 expression correlates with CD163$^+$ cell density. (a) Schematic of conditioned-medium treatment and flow cytometry: CTR or EP300-KO OCI-LY3 conditioned medium treated PMA-induced THP-1 macrophages for 48 h, then detected CD86 and CD206. (b) Representative CD86-PE/CD206-APC flow cytometry plots. (c) Quantification of CD86$^+$ and CD206$^+$ cells (CD86$^+$ = Q1+Q2, CD206$^+$ = Q2+Q3). (d) Representative multiplex immunofluorescence of DAPI/CD68/CD163/EP300 in EP300-high and EP300-low DLBCL tissues; scale bars, 20 μm. (e) Spearman correlation of EP300 MFI with CD68$^+$, CD163$^+$ and CD68$^+$CD163$^+$ cell densities in 154 DLBCL tissues; patients divided by median EP300 MFI (114.59) into high and low expression groups (n = 77 each). Data are mean ± SD from n = 3 independent experiments (b, c); two-tailed unpaired Student's t-test, ***P < 0.001; Spearman correlation test (e). CM, conditioned medium.

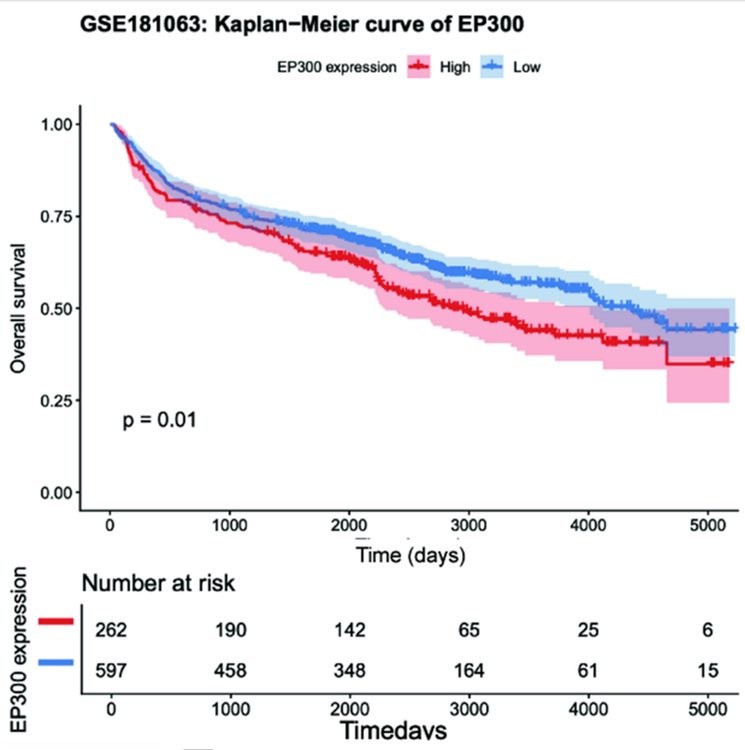
Fig. 6 Schematic diagram of the EP300–NF-κB–CXCR4 axis in macrophage M2 polarization in DLBCL. Proposed mechanism based mainly on OCI-LY3 results: EP300 knockout attenuates NF-κB-related signaling and decreases secretion of M-CSF, CCL2 and IL-10 in tumor cells, thereby impairing macrophage chemotactic response to CXCL12 and inducing a CD86-high/CD206-low phenotype.

A

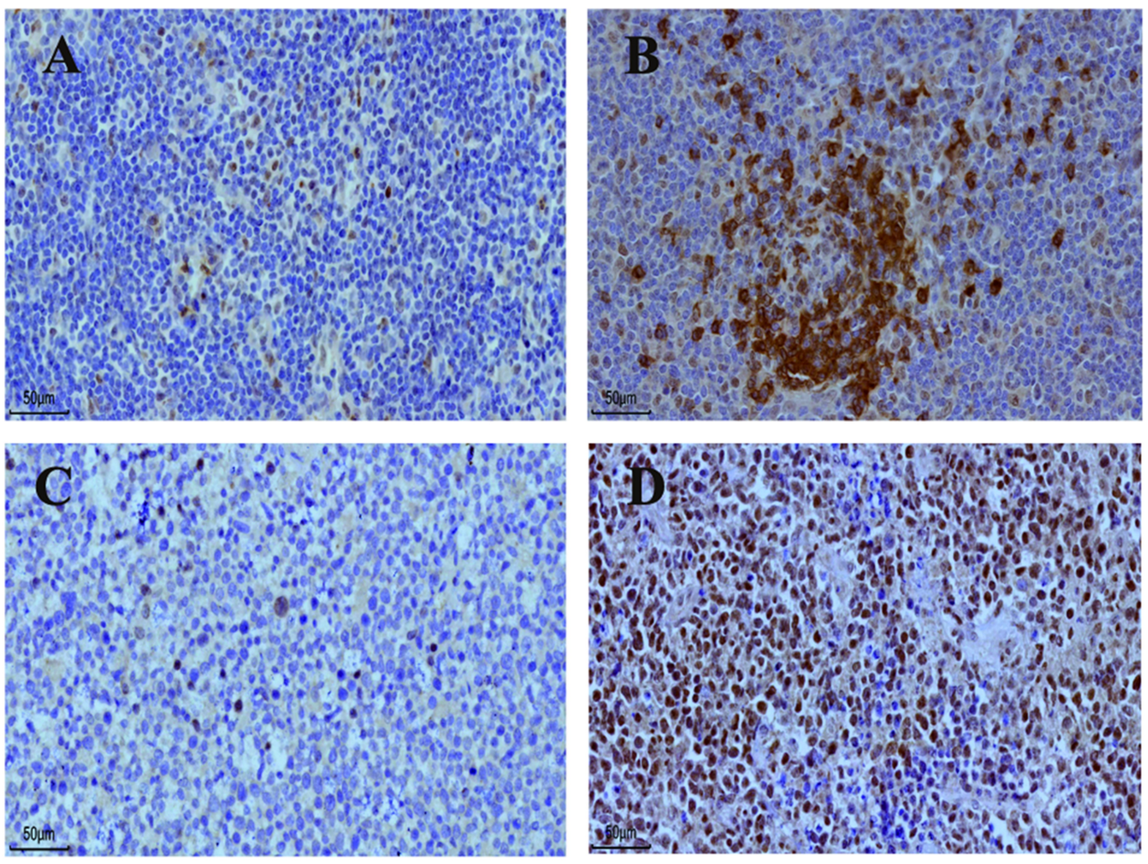

EP300 dependency in DLBCL
19 cell lines | DepMap 24Q4 Public
SU-DHL-8
OCI-LY18
U-2946
DB
SU-DHL-4
SU-DHL-10
OCI-LY-19
KARPAS-422
A3/KAW
KML-1
WILL-1
ROS-50
SU-DHL-5
HT
Farage
RI-1
RL
WSU-NHL
U-2904
-2
-1
0
CRISPR gene effect (Chronos)

B

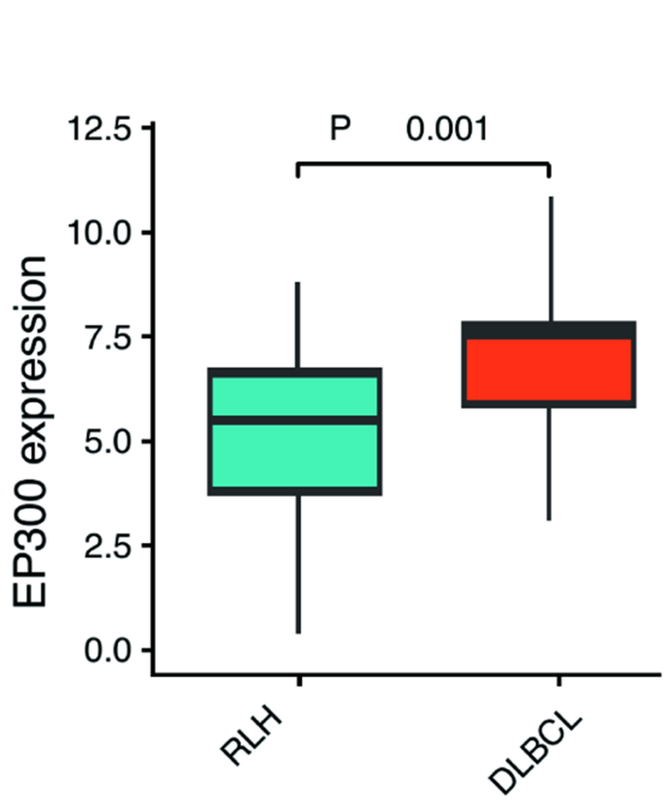

GSE10846: Kaplan–Meier curve of EP300
EP300 expression High Low
Overall survival
1.00
0.75
0.50
0.25
0.00
p = 0.0014
0
2000
4000
6000
8000
Time (days)
Number at risk
EP300 expression
221 48 11 1 0
179 20 1 1 0
Timedays


GSE181063: Kaplan–Meier curve of EP300
EP300 expression High Low
Overall survival
1.00
0.75
0.50
0.25
0.00
p = 0.01
0
1000
2000
3000
4000
5000
Time (days)
Number at risk
EP300 expression
262 190 142 65 25 6
597 458 348 164 61 15
Timedays

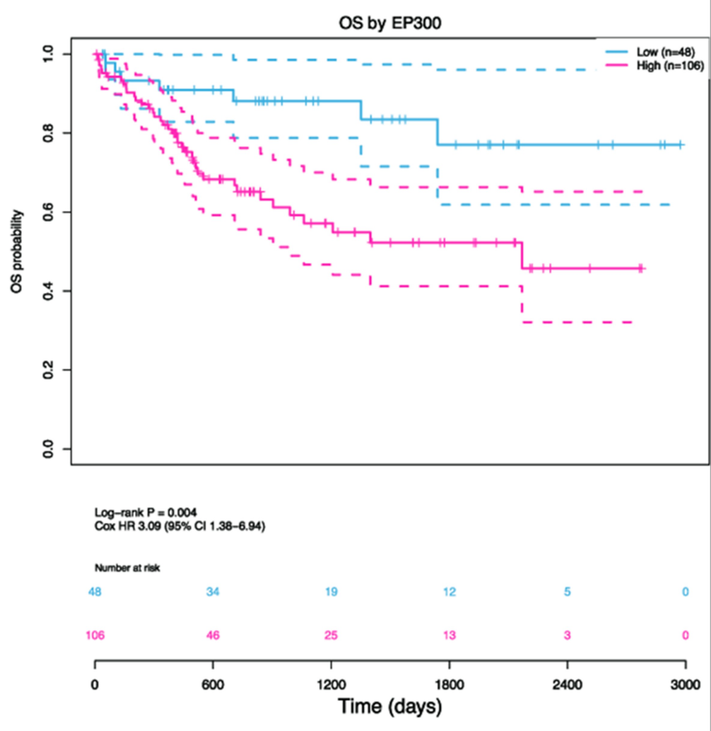
C


A
B
C
D
50μm

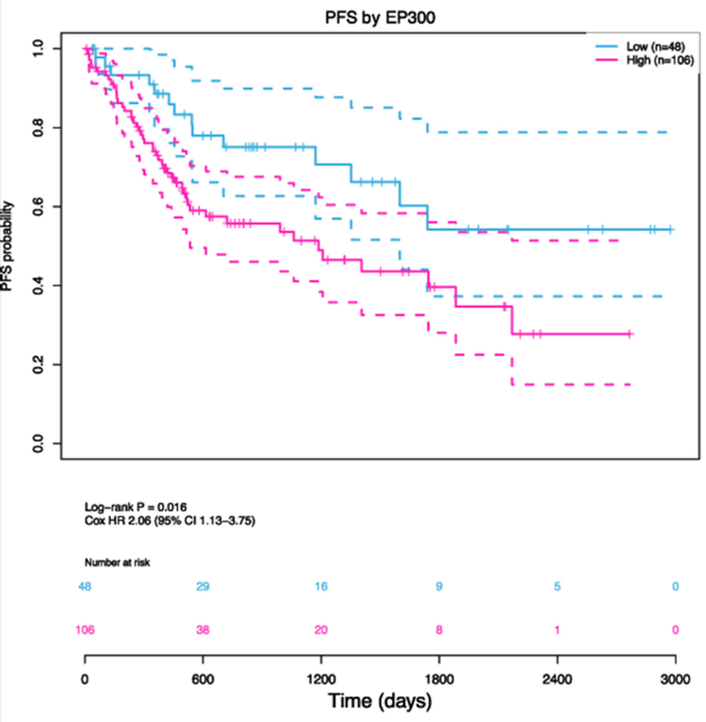
D


P 0.001
EP300 expression
12.5
10.0
7.5
5.0
2.5
0.0
RLH
DLBCL

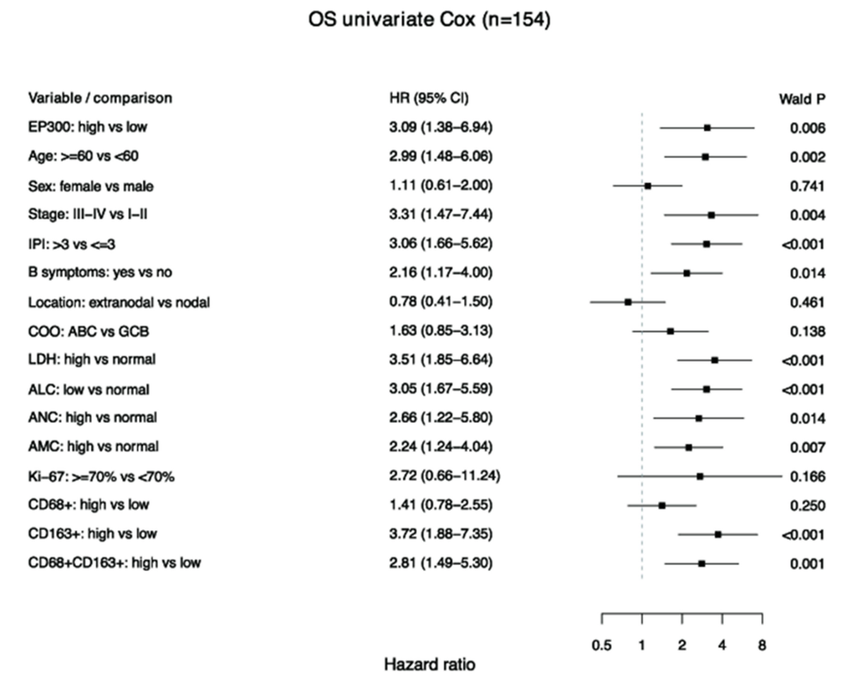
E


OS by EP300
Low (n=48)
High (n=106)
OS probability
1.0
0.8
0.6
0.4
0.2
0.0
Log-rank P = 0.004
Cox HR 3.09 (95% CI 1.38–6.94)
Number at risk
48 34 19 12 5 0
106 46 25 13 3 0
0
600
1200
1800
2400
3000
Time (days)

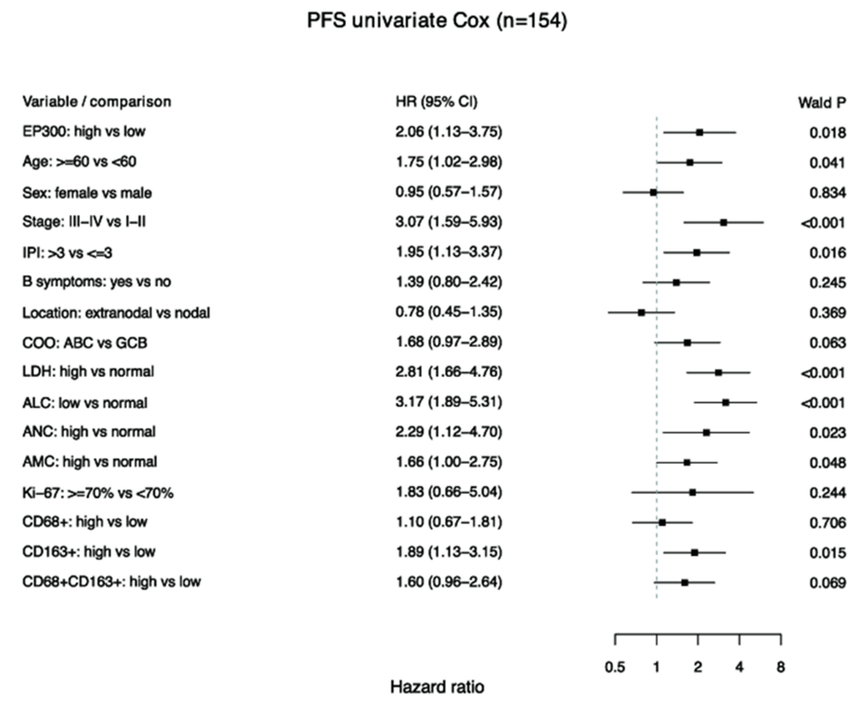
F


PFS by EP300
Low (n=48)
High (n=106)
PFS probability
1.0
0.8
0.6
0.4
0.2
0.0
Log-rank P = 0.016
Cox HR 2.06 (95% CI 1.13–3.75)
Number at risk
48 29 16 9 5 0
106 38 20 8 1 0
0
600
1200
1800
2400
3000
Time (days)

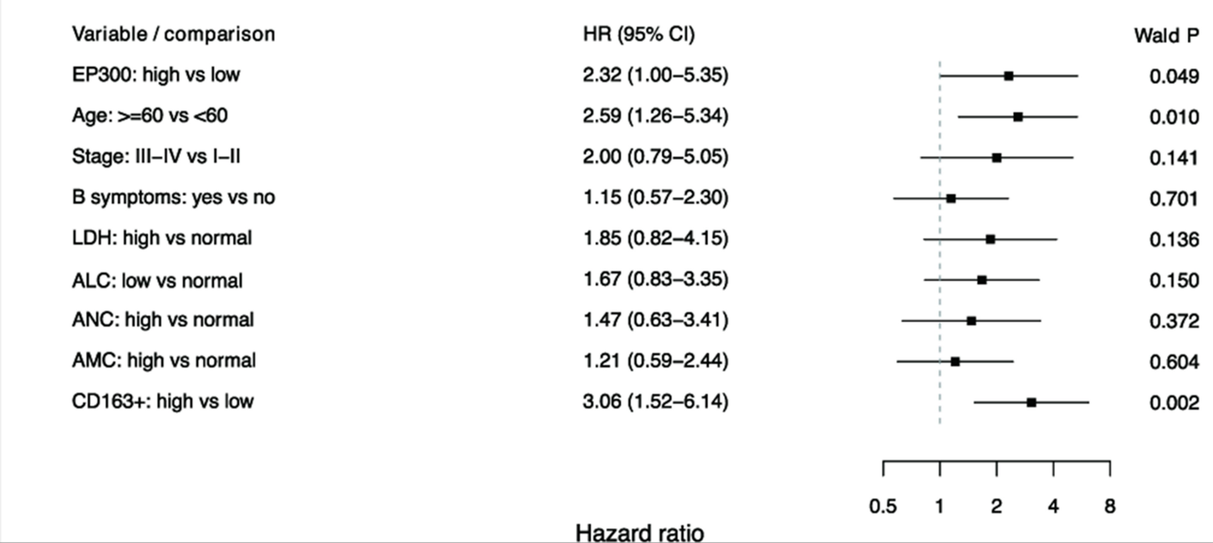
G


OS univariate Cox (n=154)
Variable / comparison
HR (95% CI)
Wald P
EP300: high vs low 3.09 (1.38–6.94) 0.006
Age: >=60 vs <60 2.99 (1.48–6.06) 0.002
Sex: female vs male 1.11 (0.61–2.00) 0.741
Stage: III–IV vs I–II 3.31 (1.47–7.44) 0.004
IPI: >3 vs <=3 3.06 (1.66–5.62) <0.001
B symptoms: yes vs no 2.16 (1.17–4.00) 0.014
Location: extranodal vs nodal 0.78 (0.41–1.50) 0.461
COO: ABC vs GCB 1.63 (0.85–3.13) 0.138
LDH: high vs normal 3.51 (1.85–6.64) <0.001
ALC: low vs normal 3.05 (1.67–5.59) <0.001
ANC: high vs normal 2.66 (1.22–5.80) 0.014
AMC: high vs normal 2.24 (1.24–4.04) 0.007
Ki–67: >=70% vs <70% 2.72 (0.66–11.24) 0.166
CD68+: high vs low 1.41 (0.78–2.55) 0.250
CD163+: high vs low 3.72 (1.88–7.35) <0.001
CD68+CD163+: high vs low 2.81 (1.49–5.30) 0.001
0.5
1
2
4
8
Hazard ratio

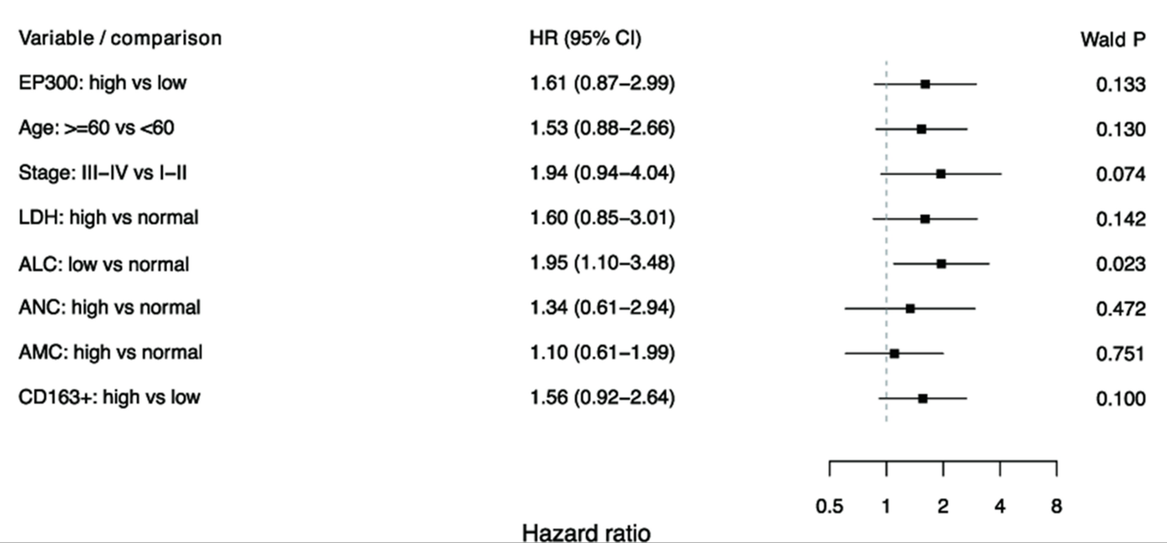
H

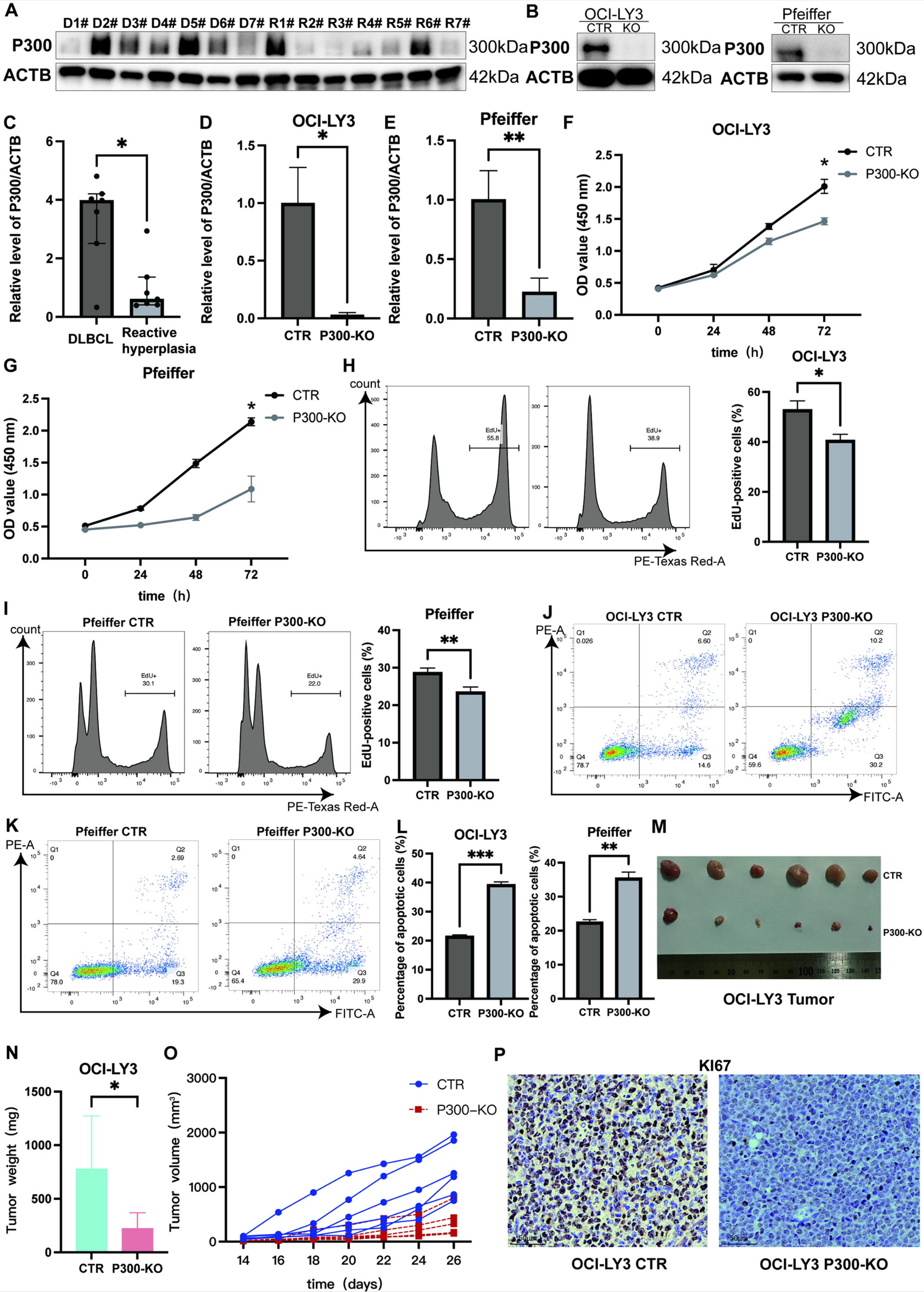

PFS univariate Cox (n=154)
Variable / comparison
HR (95% CI)
Wald P
EP300: high vs low 2.06 (1.13–3.75) 0.018
Age: >=60 vs <60 1.75 (1.02–2.98) 0.041
Sex: female vs male 0.95 (0.57–1.57) 0.834
Stage: III–IV vs I–II 3.07 (1.59–5.93) <0.001
IPI: >3 vs <=3 1.95 (1.13–3.37) 0.016
B symptoms: yes vs no 1.39 (0.80–2.42) 0.245
Location: extranodal vs nodal 0.78 (0.45–1.35) 0.369
COO: ABC vs GCB 1.68 (0.97–2.89) 0.063
LDH: high vs normal 2.81 (1.66–4.76) <0.001
ALC: low vs normal 3.17 (1.89–5.31) <0.001
ANC: high vs normal 2.29 (1.12–4.70) 0.023
AMC: high vs normal 1.66 (1.00–2.75) 0.048
Ki–67: >=70% vs <70% 1.83 (0.66–5.04) 0.244
CD68+: high vs low 1.10 (0.67–1.81) 0.706
CD163+: high vs low 1.89 (1.13–3.15) 0.015
CD68+CD163+: high vs low 1.60 (0.96–2.64) 0.069
0.5
1
2
4
8
Hazard ratio

I


OS multivariate Cox (n=154)
Variable / comparison
HR (95% CI)
Wald P
EP300: high vs low 2.32 (1.00–5.35) 0.049
Age: >=60 vs <60 2.59 (1.26–5.34) 0.010
Stage: III–IV vs I–II 2.00 (0.79–5.05) 0.141
B symptoms: yes vs no 1.15 (0.57–2.30) 0.701
LDH: high vs normal 1.85 (0.82–4.15) 0.136
ALC: low vs normal 1.67 (0.83–3.35) 0.150
ANC: high vs normal 1.47 (0.63–3.41) 0.372
AMC: high vs normal 1.21 (0.59–2.44) 0.604
CD163+: high vs low 3.06 (1.52–6.14) 0.002
0.5
1
2
4
8
Hazard ratio

J

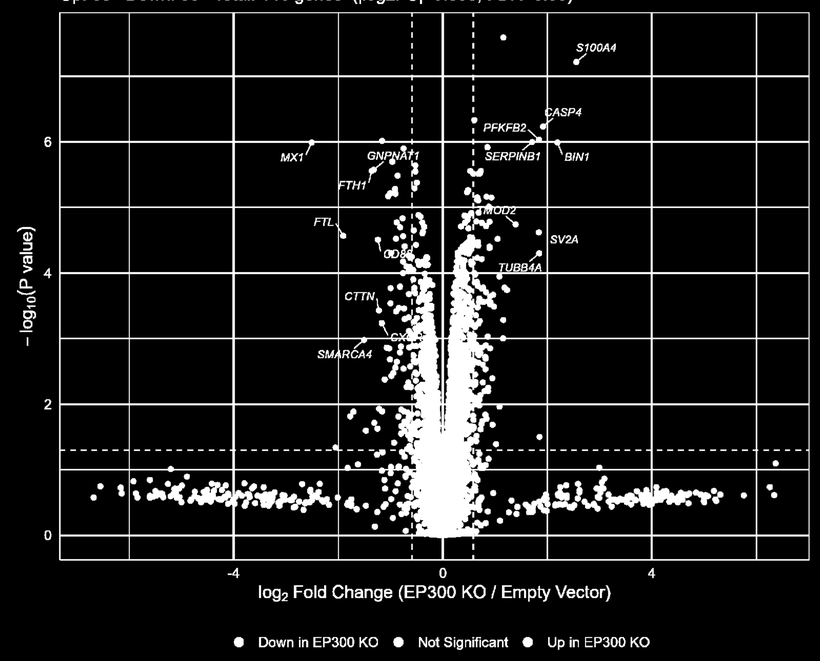

PFS multivariate Cox (n=154)
Variable / comparison
HR (95% CI)
Wald P
EP300: high vs low 1.61 (0.87–2.99) 0.133
Age: >=60 vs <60 1.53 (0.88–2.66) 0.130
Stage: III–IV vs I–II 1.94 (0.94–4.04) 0.074
LDH: high vs normal 1.60 (0.85–3.01) 0.142
ALC: low vs normal 1.95 (1.10–3.48) 0.023
ANC: high vs normal 1.34 (0.61–2.94) 0.472
AMC: high vs normal 1.10 (0.61–1.99) 0.751
CD163+: high vs low 1.56 (0.92–2.64) 0.100
0.5
1
2
4
8
Hazard ratio


A
D1# D2# D3# D4# D5# D6# D7# R1# R2# R3# R4# R5# R6# R7#
P300
ACTB
300kDa
42kDa
B
OCI-LY3
CTR KO
Pfeiffer
CTR KO
P300
ACTB
300kDa
42kDa
C
Relative level of P300/ACTB
DLBCL
Reactive hyperplasia
D
OCI-LY3
Relative level of P300/ACTB
CTR P300-KO
E
Pfeiffer
Relative level of P300/ACTB
CTR P300-KO
F
OCI-LY3
CTR
P300-KO
OD value (450 nm)
time (h)
G
Pfeiffer
CTR
P300-KO
OD value (450 nm)
time (h)
H
count
EdU+ 55.8
EdU+ 38.9
PE-Texas Red-A
EdU-positive cells (%)
CTR P300-KO
I
Pfeiffer CTR
Pfeiffer P300-KO
count
EdU+ 30.1
EdU+ 22.0
PE-Texas Red-A
Pfeiffer
EdU-positive cells (%)
CTR P300-KO
J
OCI-LY3 CTR
OCI-LY3 P300-KO
PE-A
Q1 0.026
Q2 6.60
Q4 78.7
Q3 14.6
Q1 0
Q2 10.2
Q4 59.6
Q3 30.2
FITC-A
K
Pfeiffer CTR
Pfeiffer P300-KO
PE-A
Q1 0
Q2 2.69
Q4 78.0
Q3 19.3
Q1 0
Q2 4.64
Q4 65.4
Q3 29.9
FITC-A
L
OCI-LY3
Percentage of apoptotic cells (%)
CTR P300-KO
Pfeiffer
Percentage of apoptotic cells (%)
CTR P300-KO
M
CTR
P300-KO
OCI-LY3 Tumor
N
OCI-LY3
Tumor weight (mg)
CTR P300-KO
O
CTR
P300–KO
Tumor volume (mm³)
time (days)
P
KI67
OCI-LY3 CTR
OCI-LY3 P300-KO
50μm

A

Volcano Plot: EP300 KO vs Empty Vector (Gene-level)

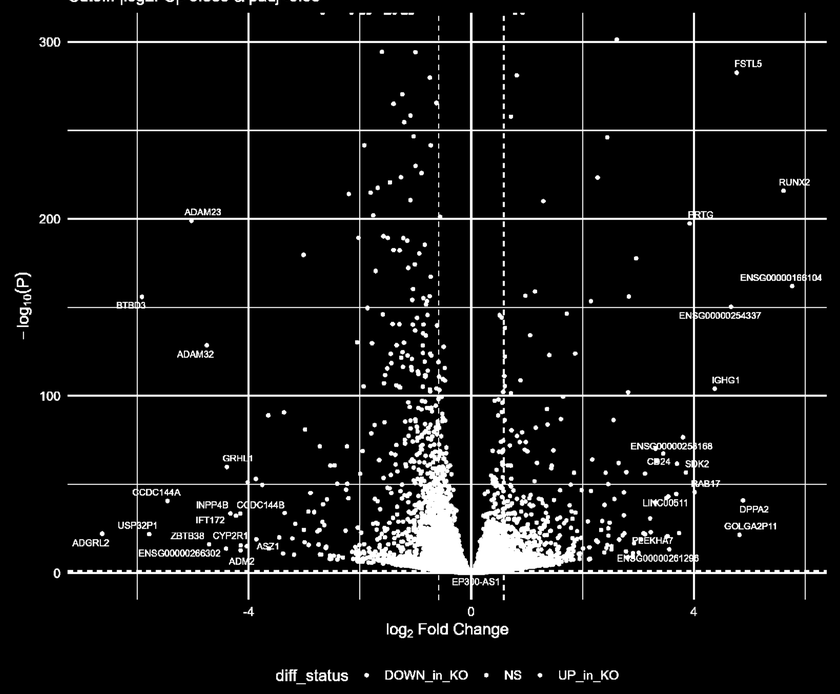
Up: 88 Down: 58 Total: 146 genes (|log2FC|>0.585, FDR<0.05)



B

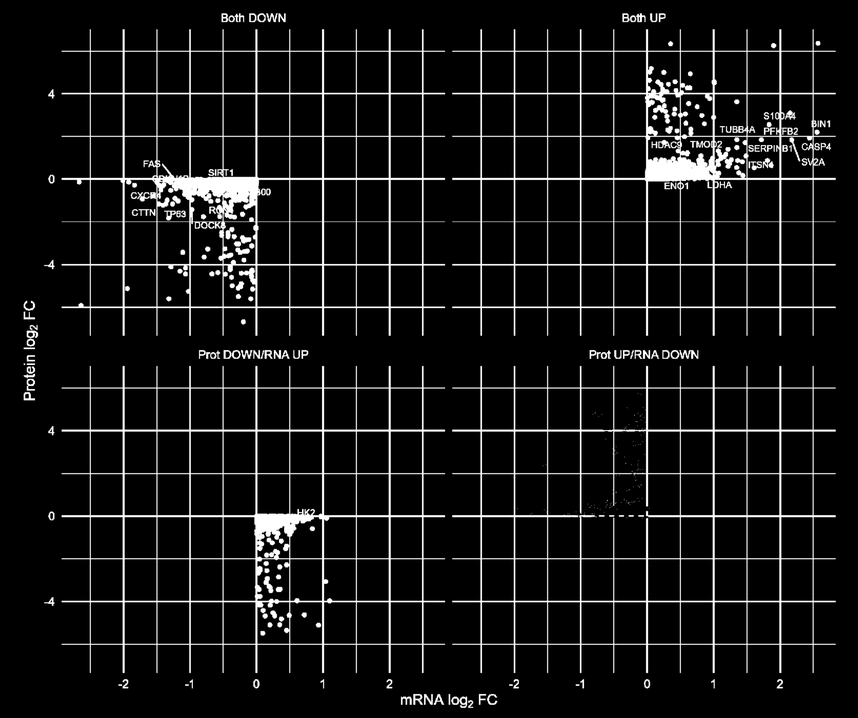
RNA-seq: EP300 KO vs EC (↑1199 ↓1296)

Cutoff: |log2FC|>0.585 & padj<0.05



C

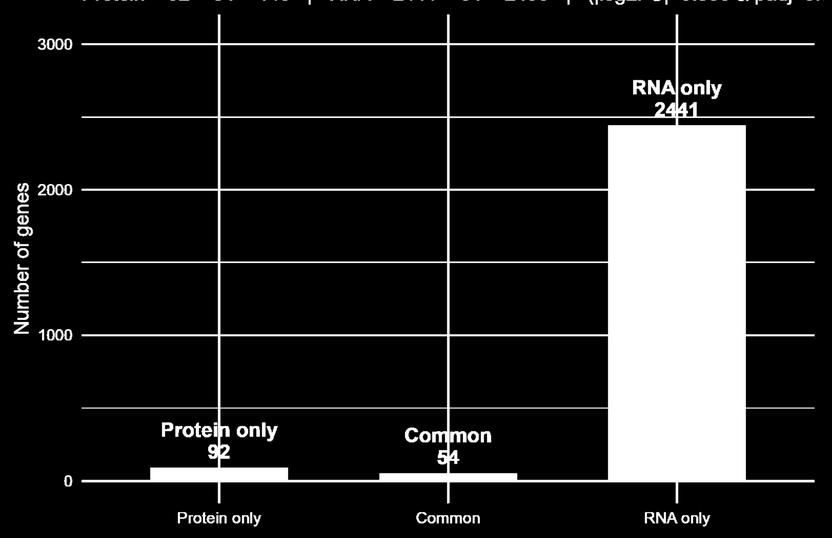
Four-Quadrant: Protein vs mRNA



D

DE Genes: Protein vs RNA (Gene-level)

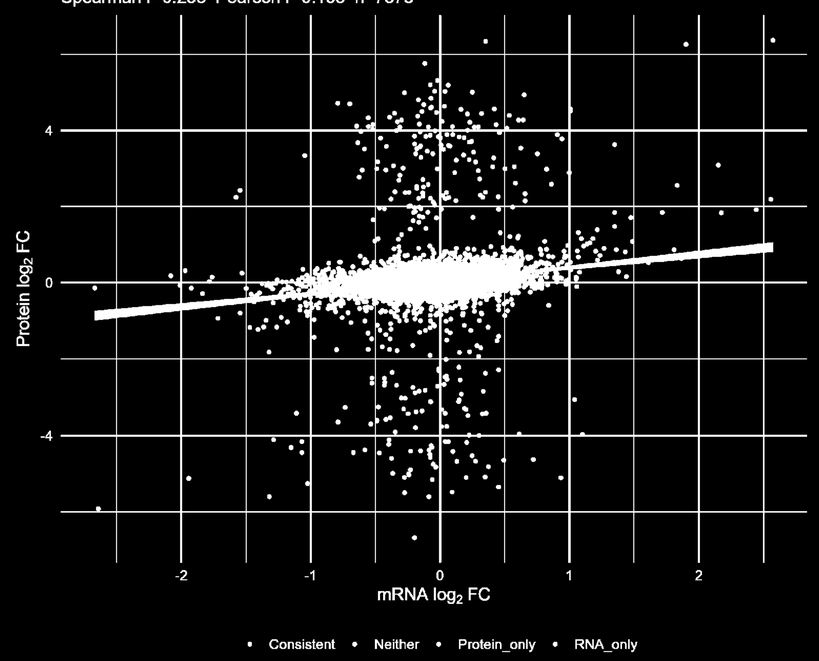
Protein = 92 + 54 = 146 | RNA = 2441 + 54 = 2495 | (|log2FC|>0.585 & padj<0.(



E

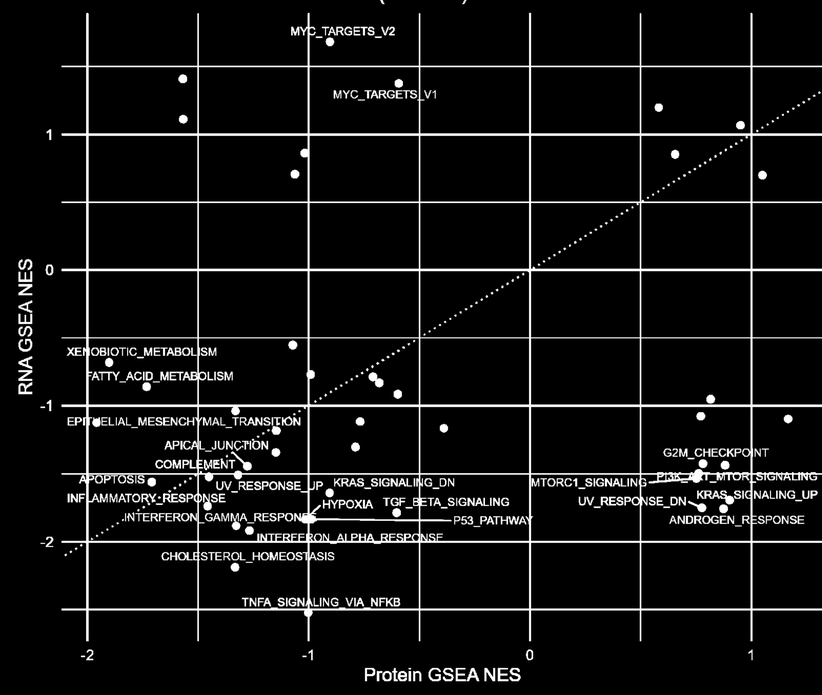
Protein vs mRNA Fold Change

Spearman r=0.238 Pearson r=0.163 n=7578

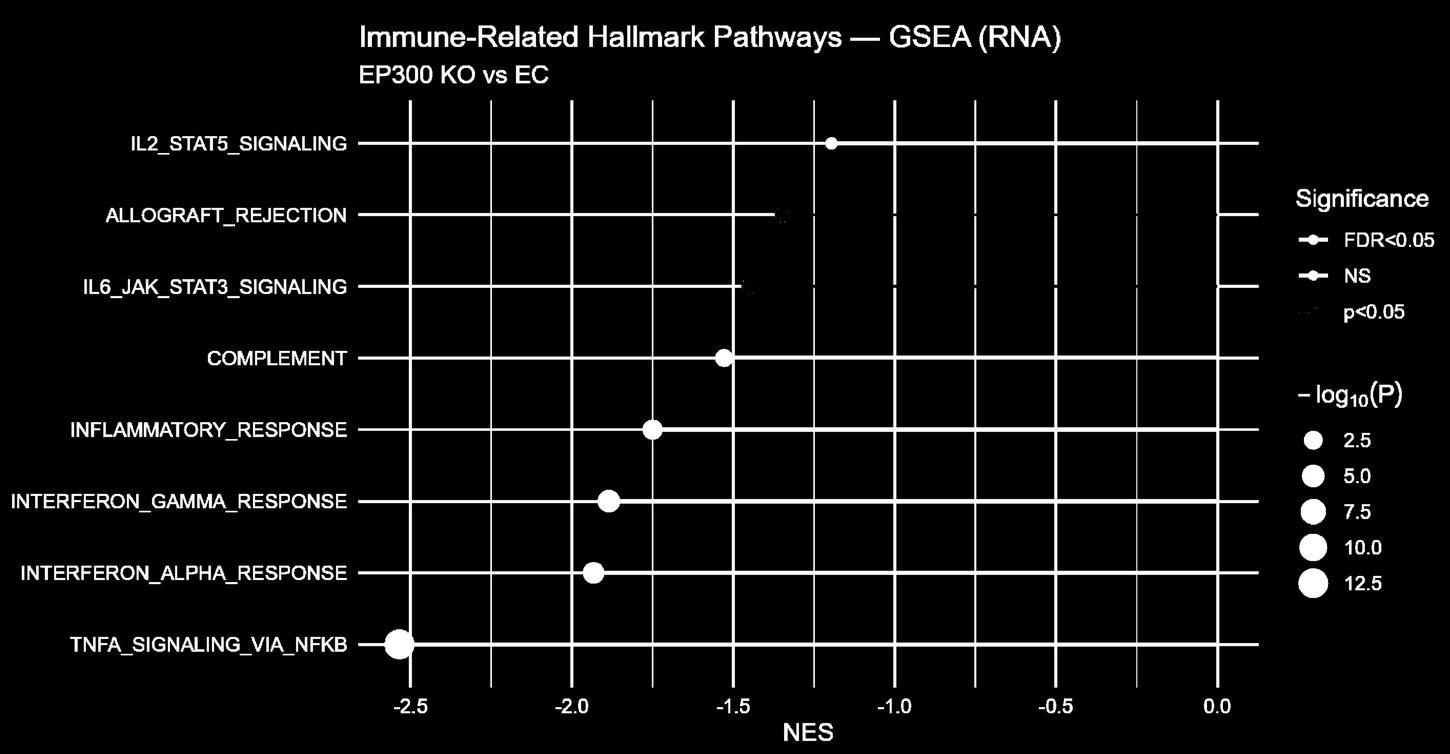


F

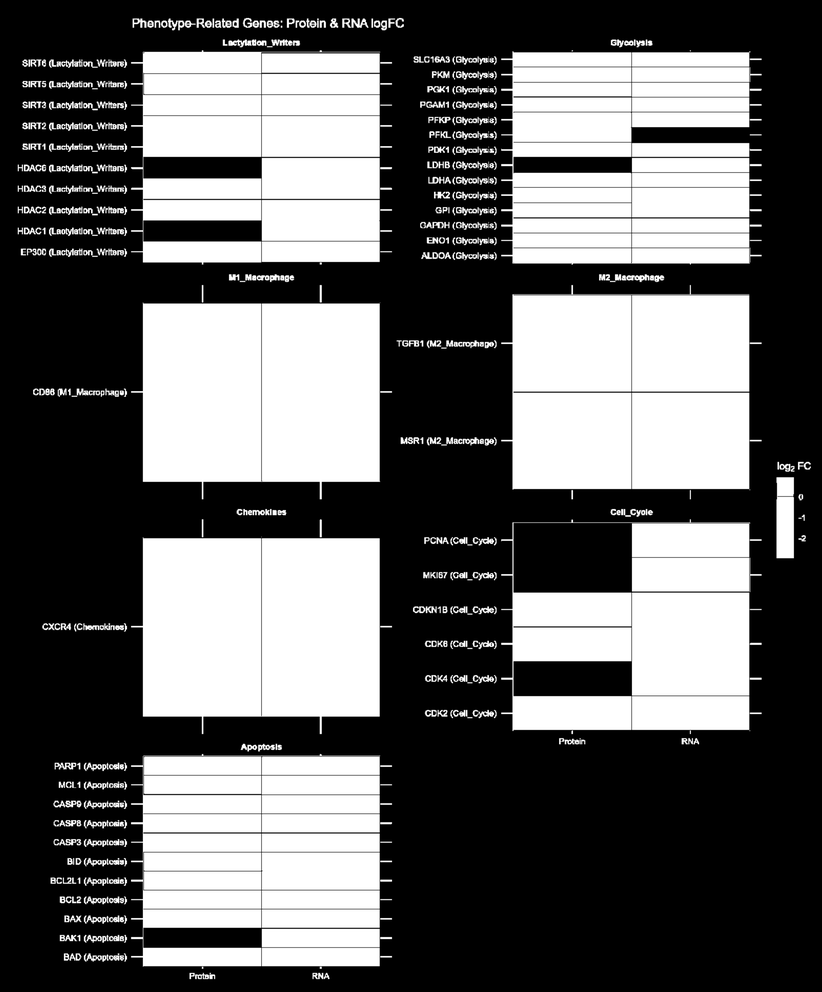
Hallmark NES: Protein vs RNA (r=0.065)



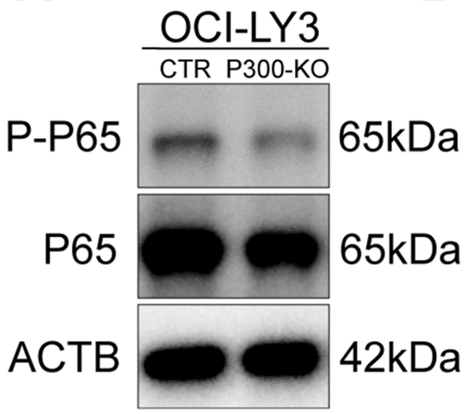
G



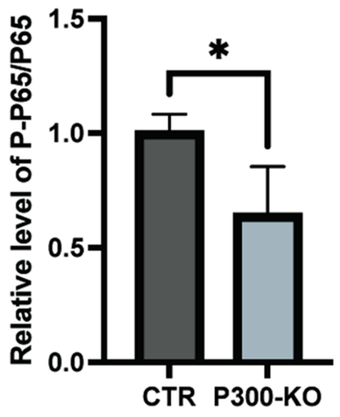
H



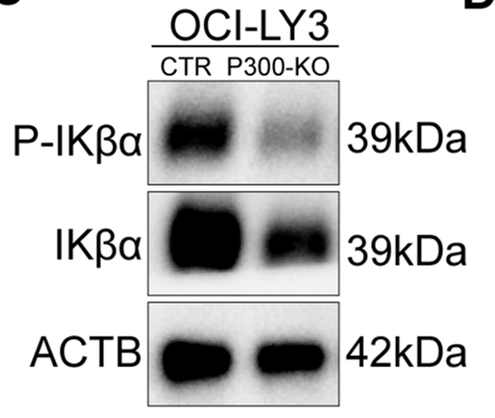
A


OCI-LY3
CTR P300-KO
P-P65
65kDa
P65
65kDa
ACTB
42kDa

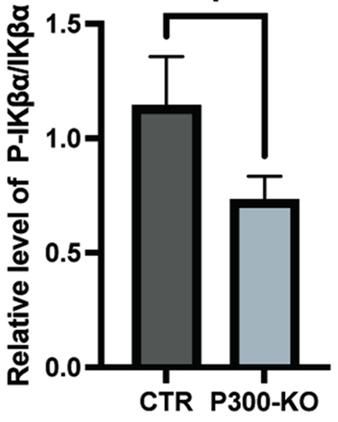
B


Relative level of P-P65/P65
1.5
1.0
0.5
0.0
*
CTR P300-KO

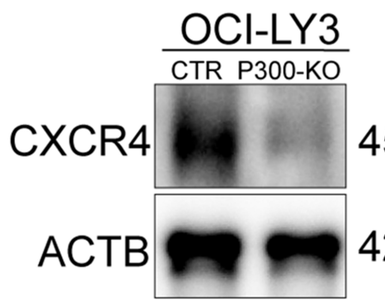
C


OCI-LY3
CTR P300-KO
P-IKβα
39kDa
IKβα
39kDa
ACTB
42kDa

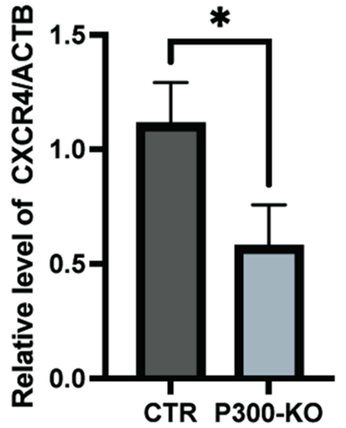
D


Relative level of P-IKβα/IKβα
1.5
1.0
0.5
0.0
*
CTR P300-KO

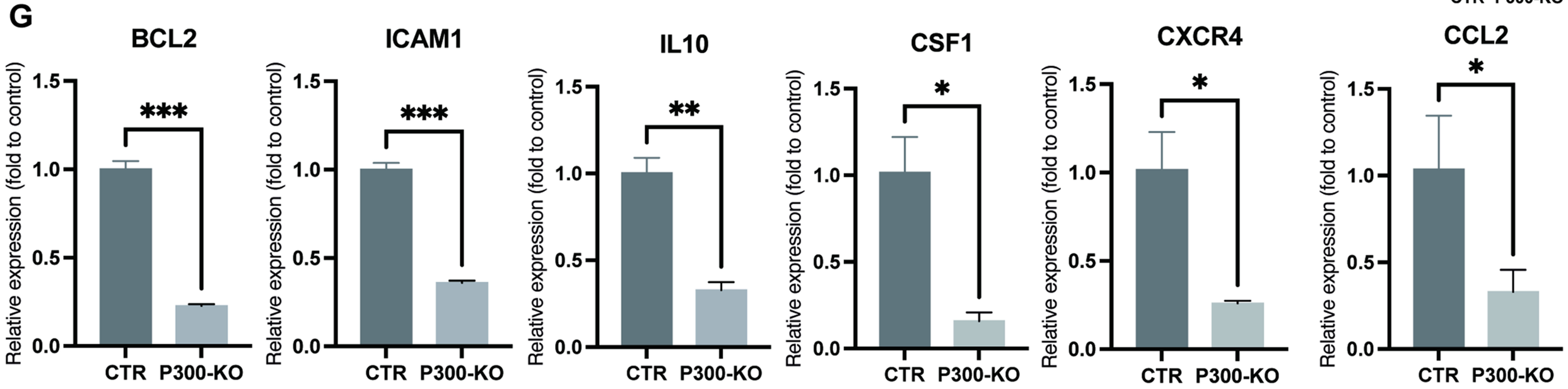
E


OCI-LY3
CTR P300-KO
CXCR4
45kDa
ACTB
42kDa

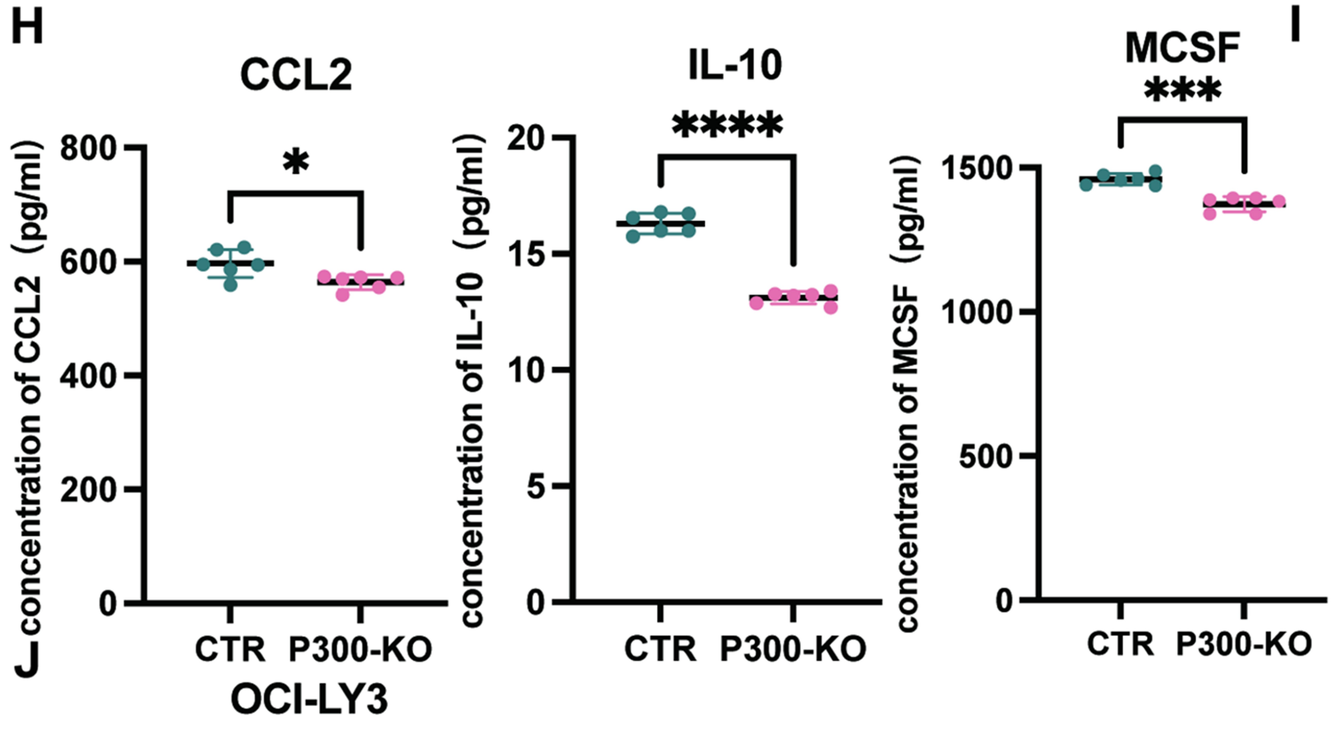
F


Relative level of CXCR4/ACTB
1.5
1.0
0.5
0.0
*
CTR P300-KO

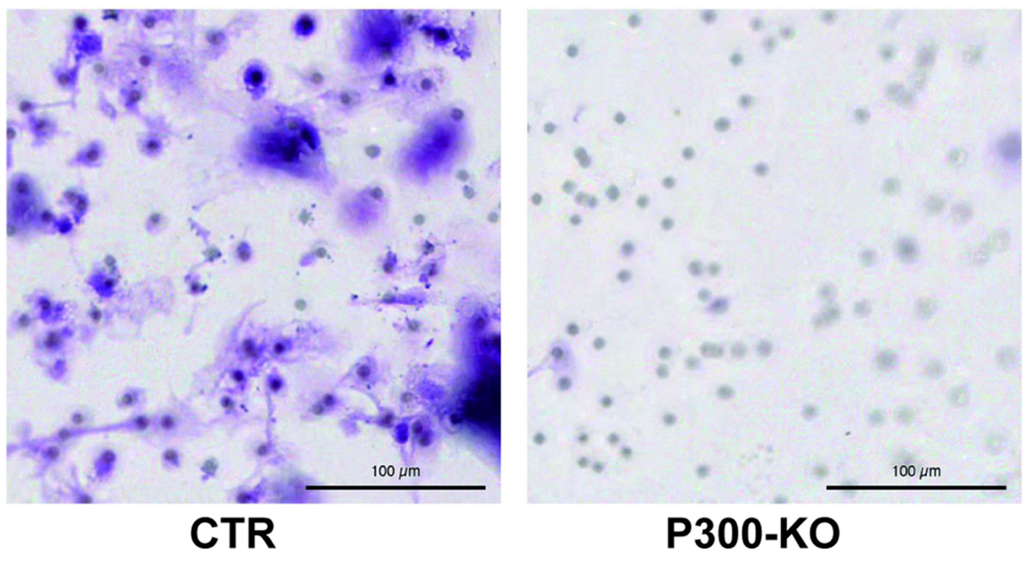
G

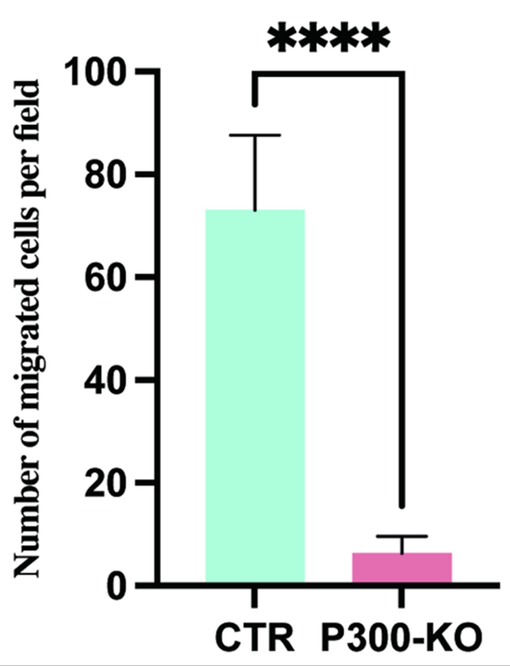

BCL2
ICAM1
IL10
CSF1
CXCR4
CCL2
Relative expression (fold to control)
1.5
1.0
0.5
0.0
***
**
*
CTR P300-KO

H

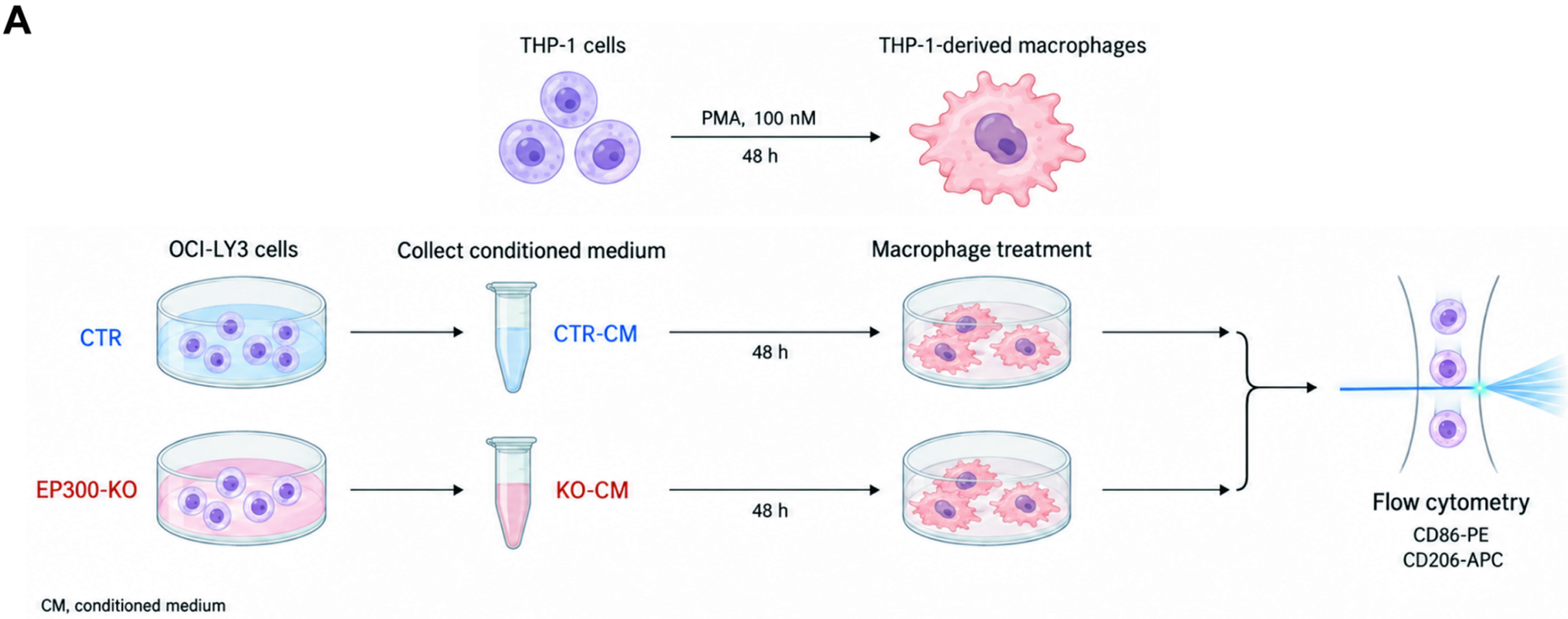

CCL2
concentration of CCL2 (pg/ml)
800
600
400
200
0
*
CTR P300-KO
IL-10
concentration of IL-10 (pg/ml)
20
15
10
5
0
****
CTR P300-KO
MCSF
concentration of MCSF (pg/ml)
1500
1000
500
0
***
CTR P300-KO

I

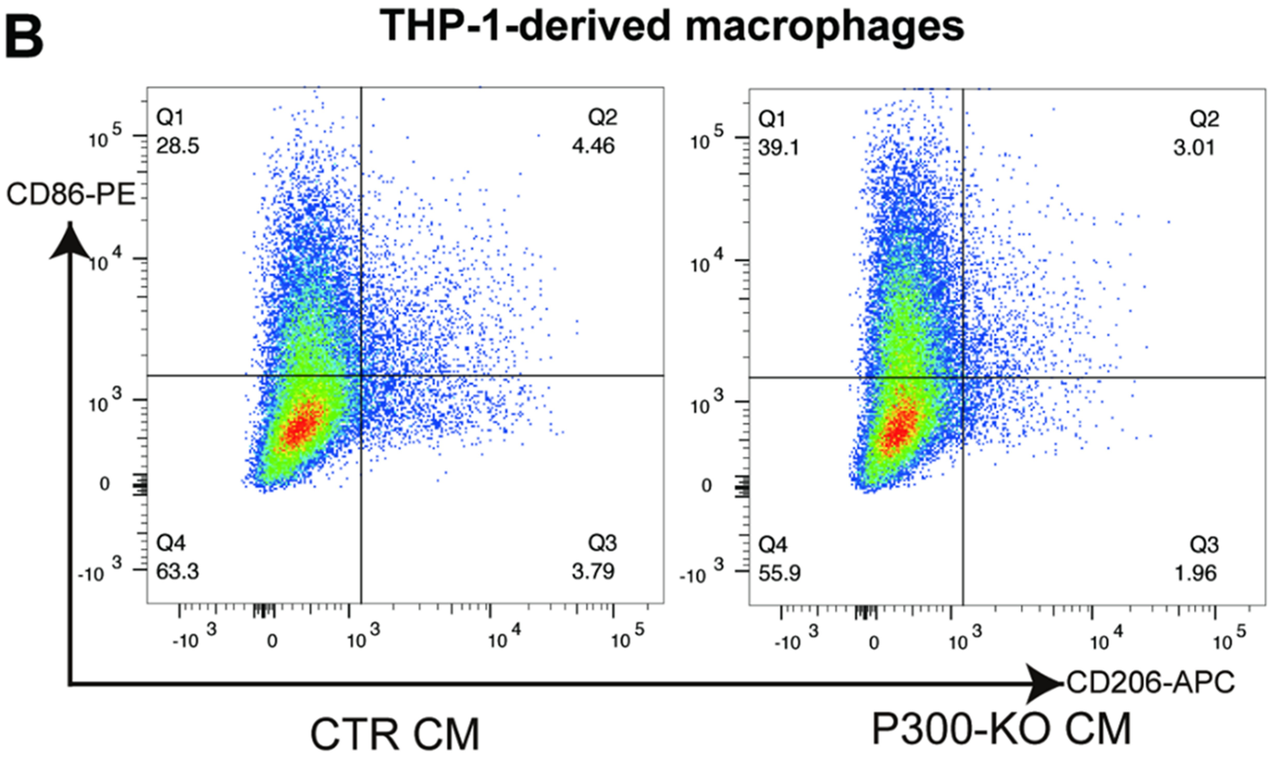

OCI-LY3
100 μm
CTR
100 μm
P300-KO


OCI-LY3
Number of migrated cells per field
100
80
60
40
20
0
****
CTR P300-KO

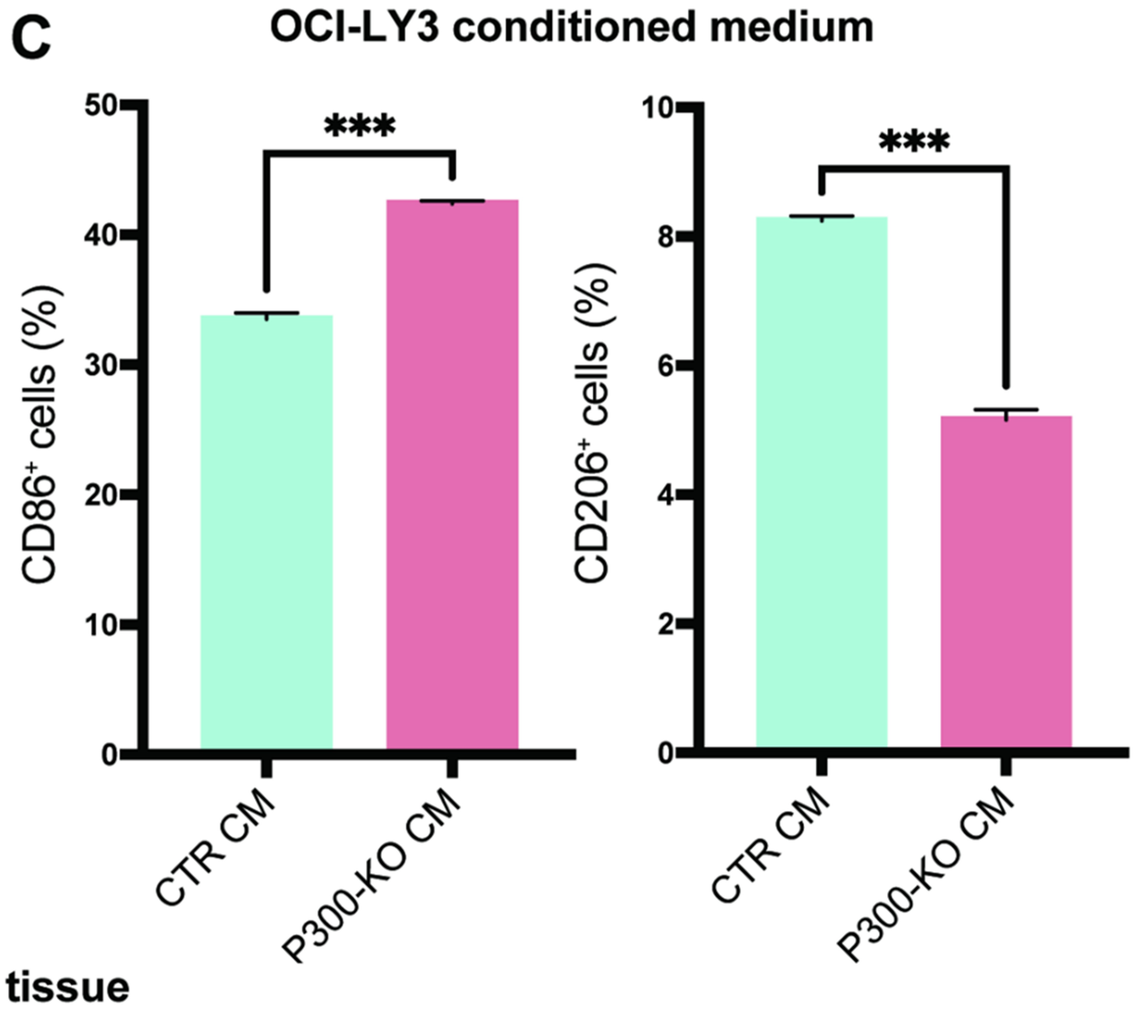
A


THP-1 cells
THP-1-derived macrophages
PMA, 100 nM
48 h
OCI-LY3 cells
Collect conditioned medium
Macrophage treatment
CTR
CTR-CM
48 h
EP300-KO
KO-CM
48 h
Flow cytometry
CD86-PE
CD206-APC
CM, conditioned medium

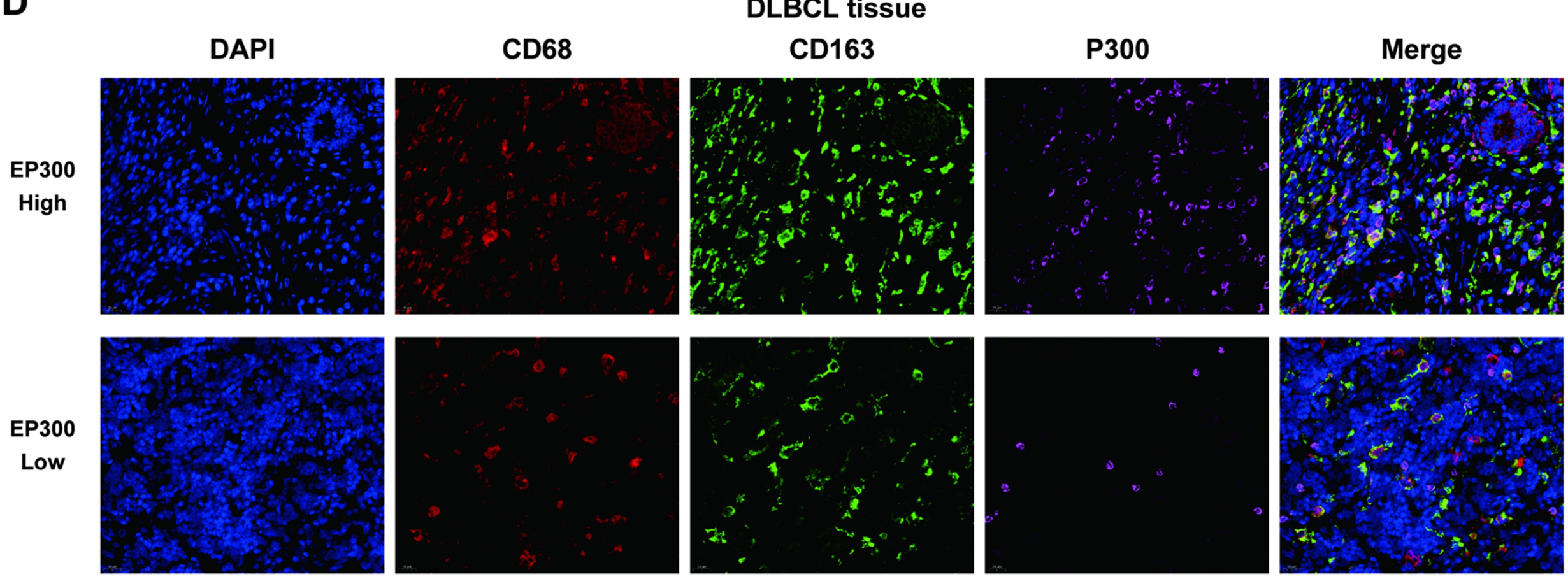
B


THP-1-derived macrophages
Q1
28.5
Q2
4.46
Q4
63.3
Q3
3.79
Q1
39.1
Q2
3.01
Q4
55.9
Q3
1.96
CD86-PE
CD206-APC
CTR CM
P300-KO CM

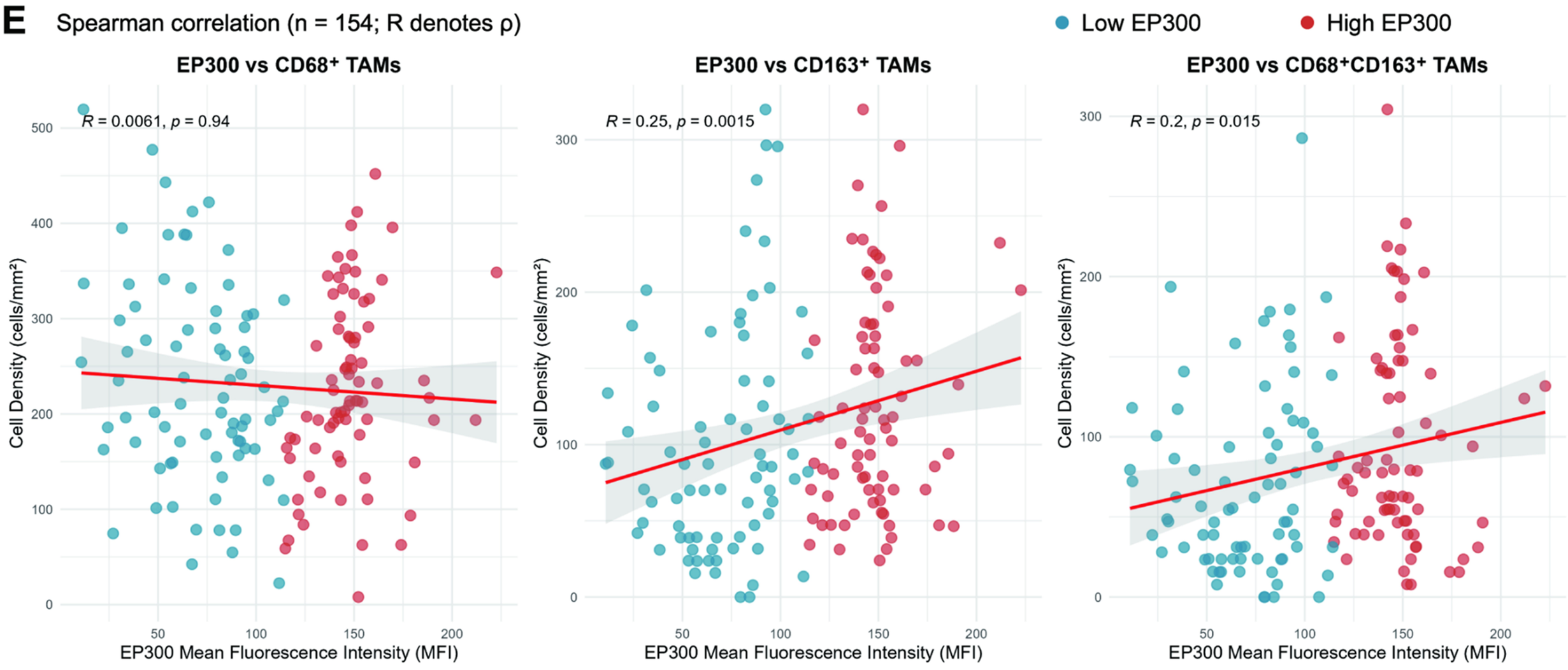
C


OCI-LY3 conditioned medium
CD86⁺ cells (%)
CD206⁺ cells (%)
***
***
CTR CM
P300-KO CM
CTR CM
P300-KO CM

D


DLBCL tissue
DAPI
CD68
CD163
P300
Merge
EP300 High
EP300 Low

E


Spearman correlation (n = 154; R denotes ρ)
Low EP300
High EP300
EP300 vs CD68⁺ TAMs
EP300 vs CD163⁺ TAMs
EP300 vs CD68⁺CD163⁺ TAMs
R = 0.0061, p = 0.94
R = 0.25, p = 0.0015
R = 0.2, p = 0.015
Cell Density (cells/mm²)
EP300 Mean Fluorescence Intensity (MFI)

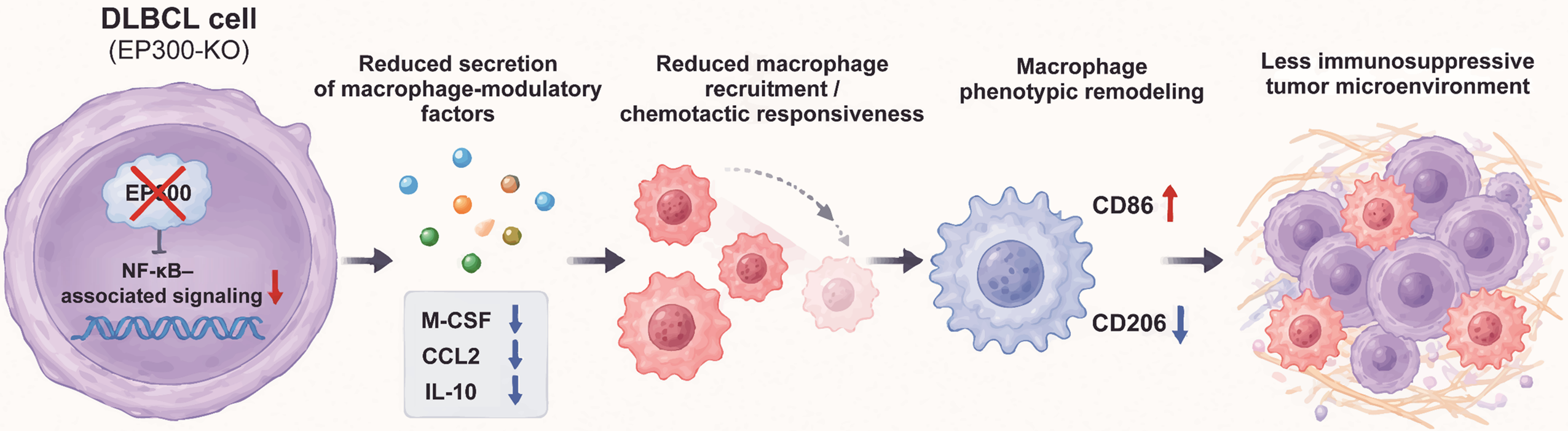

DLBCL cell
(EP300-KO)
EP300
NF-κB–
associated signaling
Reduced secretion
of macrophage-modulatory
factors
M-CSF
CCL2
IL-10
Reduced macrophage
recruitment /
chemotactic responsiveness
Macrophage
phenotypic remodeling
CD86
CD206
Less immunosuppressive
tumor microenvironment

Table 1 Expression of EP300 in DLBCL and RLH tissues [n (%)]

Group	N	EP300 low expression	EP300 high expression	χ^2	*P*
RLH	93	67（72.04%）	26（27.96%）	38.93	**＜0.001**
DLBCL	154	48（31.17%）	106（68.83%）		

Table 2 Relationship between EP300 expression and clinical features of DLBCL patients[n(%)]

Clinical features	N	EP300 low expression	EP300 high expression	χ^2	*P*
Age					
＜60 years	62	21（33.87%）	41（66.13%）	0.353	0.552
≥60 years	92	27（29.35%）	65（70.65%）		
Sex					
Male	68	18（26.47%）	50（73.53%）	1.253	0.263
Female	86	30（34.88%）	56（65.12%）		
Ann Arbor Stage					
I-II	50	17（34.00%）	33（66.00%）	0.277	0.599
III-IV	104	31（29.81%）	73（70.19%）		
IPI Score					
≤3	111	38（34.23%）	73（65.77%）	1.741	0.187
＞3	43	10（23.26%）	33（76.74%）		
B Symptoms					
No	111	37（33.33%）	74（66.67%）	0.868	0.351
Yes	43	11（25.58%）	32（74.42%）		
Location					
Nodal	107	37（34.58%）	70（65.42%）	1.901	0.168
Extranodal	47	11（23.40%）	36（76.60%）		
COO classification					
GCB	58	24（41.38%）	34（58.62%）	4.521	0.033
ABC	96	24（25.00%）	72（75.00%）		

Clinical features	N	EP300 low expression	EP300 high expression	χ^2	*P*
LDH levels					
Normal	80	28（35.00%）	52（65.00%）	1.139	0.286
High	74	20（27.03%）	54（72.97%）		
ALC					
Normal	91	37（40.66%）	54（59.34%）	9.339	0.002
Low	63	11（17.46%）	52（82.54%）		
ANC					
Normal	137	43（31.39%）	94（68.61%）	0.027	0.868
High	17	5（29.41%）	12（70.59%）		
AMC					
Normal	94	29（30.85%）	65（69.15%）	0.011	0.915
High	60	19（31.67%）	41（68.33%）		
Ki67 expression					
＜70%	16	6（37.50%）	10（62.50%）	/	0.576*
≥70%	138	42（30.43%）	96（69.57%）		

*Fisher's exact test was used.

Table 3. Descriptive statistics of multiplex immunofluorescence measurements in 154 patients with DLBCL

Variable	N	Median (Q1, Q3)	Mean ± SD
EP300 MFI	154	114.59 (76.75, 147.34)	109.15 ± 45.74
CD68+TAMs	154	213.62 (163.84, 296.52)	228.81 ± 100.25
CD163+TAMs	154	93.74 (54.83, 162.2)	113.04 ± 73.23
CD68+CD163+TAMs	154	64.63 (35.44, 123.92)	83.19 ± 62.21

Data are presented as median (Q1, Q3) and mean ± SD. Each variable was available for all 154 patients. EP300 MFI denotes mean fluorescence intensity. $CD68^+$, $CD163^+$, and $CD68^+CD163^+$ TAM densities are expressed as cells/mm^2. $CD68^+CD163^+$ TAMs denote double-positive tumor-associated macrophages. For survival analyses, the three TAM density variables were dichotomized according to their respective medians, and the high/low classifications recorded in the source dataset were used; the low group served as the reference. EP300 expression determined by immunohistochemistry and EP300 MFI measured by multiplex immunofluorescence were analyzed as distinct variables.

Supplementary Files

This is a list of supplementary files associated with this preprint. Click to download.

- P300rawdataWB.zip
- supplementdata.docx